Journal of Wind Engineering & Industrial Aerodynamics 180 (2018) 66–87

Contents lists available at ScienceDirect

Journal of Wind Engineering & Industrial Aerodynamics

journal homepage: www.elsevier.com/locate/jweia

A review of computational fluid dynamics (CFD) simulations of the wind flow around buildings for urban wind energy exploitation

Francisco Toja-Silva [a,b,*], Takaaki Kono [c], Carlos Peralta [d], Oscar Lopez-Garcia [e], Jia Chen [a]

[a] Environmental Sensing and Modeling, Technische Universität München (TUM), Theresienstr. 90, Munich, 80333, Germany
[b] Barcelona Supercomputing Center (BSC), Nexus II Building - Jordi Girona 29, 08034, Barcelona, Spain
[c] Research Center for Sustainable Energy and Technology, Kanazawa University, Natural Science and Technology Hall 3, 3B416 Kakuma-machi, Kanazawa-shi, Ishikawa, 920-1192, Japan
[d] Wobben Research and Development Management Support GmbH, Teerhof 59, Bremen, 28199, Germany
[e] Escuela Técnica Superior de Ingenieros Aeronáuticos, Universidad Politécnica de Madrid, Pl. Cardenal Cisneros 3, Madrid, 28040, Spain

ARTICLE INFO

Keywords:
Building aerodynamics
CFD
Computational wind engineering
LES
RANS
Urban wind energy

ABSTRACT

This article presents a review on computational fluid dynamics (CFD) applied to urban wind energy exploitation. The content comprises technical CFD aspects relevant for this application and the current state-of-the-art in building aerodynamics applied to urban wind energy. The majority of studies (more than 50% of the respective criteria) used Reynolds-averaged Navier-Stokes (RANS) turbulence models, the commercial solver ANSYS, simulated a full-scale geometry and studied an isolated building. For RANS, at least second order-accurate discretization schemes must be used, to improve turbulence kinetic energy prediction. In large-eddy simulation (LES) studies, a blending scheme is often needed to avoid numerical instability. Urban wind flow is very complex (i.e. detachment, stagnation), and rigorous validation and verification processes are needed, because only sophisticated turbulence models are able to yield acceptable results. The building-roof shape was optimized for the wind energy exploitation attending to both turbulence intensity and wind velocity. Conventional roof and roof edge shapes were studied, as well as the compatibility with the installation of solar panels. Wind turbines sitting was also discussed. Few simulations of wind turbines installed on building roofs were conducted using wind turbine models, whereas real geometries of vertical axis wind turbines were simulated and optimized.

1. Introduction

The total amount of wind energy power is augmenting exponentially in the World, mainly thanks to large wind turbines (Toja-Silva et al., 2013). However, small wind turbines in urban areas are still mostly unused, what supposes a waste of a significant energy resource (Walker, 2011). As it is well known, distributed energy generation (generation at the consumption site) offers significant benefits in terms of high energy efficiency, lower emission of pollutants, reduced energy dependence and stimulation of the economy (Chicco and Mancarella, 2009). Micro wind generation in the urban environment is viable. The major barriers are social perception of noise and visual acuity, concerns about safety, and the relative high cost and maintenance of small wind turbines compared with other easier and more robust alternatives, e.g. photovoltaics (Encraft, 2009).

Toja-Silva et al. (2013) reviewed the opportunities and challenges for urban wind energy exploitation showing the potential of such an energy source, but also pointed out another impediment, a certain lack of societal acceptance due to the customers' disappointment regarding the difference between the expected and the real energy generated. A careful analysis of the wind flow around buildings is needed, in order to decide the best possible positioning for wind turbines to take advantage of the accelerating effect of the wind on the roof, and the most adequate kind of wind turbine for such particular case. Computational fluid dynamics (CFD) is the best tool existing nowadays to carry out a careful analysis of the wind flow around buildings. This field of study is called building aerodynamics. Several investigations carried out CFD simulations of the wind in urban environments, e.g. pedestrian comfort (Blocken and Carmeliet, 2008; Blocken et al., 2016; Du et al., 2017) and pollutant dispersion (Nozu and Tamura, 2012; Tominaga and Stathopoulos, 2013). Toja-Silva et al. (2017, 2018) also used CFD to simulate the column-averaged greenhouse gas concentrations (Chen et al., 2016) in an

* Corresponding author. Barcelona Supercomputing Center (BSC), Nexus II Building - Jordi Girona 29, 08034 Barcelona, Spain.
E-mail address: frantojasilva@yahoo.es (F. Toja-Silva).

https://doi.org/10.1016/j.jweia.2018.07.010
Received 28 March 2018; Received in revised form 28 June 2018; Accepted 14 July 2018
Available online 23 July 2018

urban area and utilized real measurements to verify the results. In the present review, however, we focus on urban wind energy.

Walker (2011) reviews methods of estimating urban wind resource including a short section about the use of CFD. Few articles were cited about CFD applied to urban wind energy. A significant part of the discussion focuses on ducted wind turbines. Millward-Hopkins et al. (2013) mapped the wind resource over UK cities using statistical methods, and stated that "detailed CFD studies would be required in order to obtain detailed flow information around individual rooftops". Toja-Silva et al. (2013) conducted CFD simulations of the wind flow around a simple building to qualitatively assess the effect on wind turbines of the highly variable wind conditions on a building roof. This review includes some studies on CFD simulations, but the main focus was on the opportunities and challenges of the urban wind energy technology. Blocken (2014) published a widely cited review article about computational wind engineering (probably the most important review up to the date), stressing the need of a review article about CFD applied to urban wind energy.

The present article is aimed at providing a review about the state-of-the-art of CFD applied to urban wind energy resource assessment. In what follows, Section 2 is a technical section that discusses the turbulence modelling, numerical schemes, meshing and the best practice guidelines used for the CFD simulation of the urban wind for wind energy exploitation purposes. Section 3 focuses on application, and shows previous investigations reported in the literature regarding the simulation of the wind on isolated building roofs and build environments. Section 4 focuses on the simulation of wind turbines (using both models and real geometries) on building roofs. Finally, a summary is presented in Section 5.

2. Computational modelling of the urban wind

2.1. Turbulence modelling

2.1.1. Reynolds-averaged Navier-Stokes (RANS)

The RANS equations (mass and momentum conservation) for incompressible fluids without body forces (Cheng et al., 2003) are normally used for urban wind energy applications, i.e.

$$\frac{\partial \overline{u}_i}{\partial x_i} = 0 \tag{1}$$

and

$$\frac{\partial\left(\overline{u}_i \overline{u}_j\right)}{\partial x_j} = -\frac{1}{\rho}\frac{\partial \overline{p}}{\partial x_i} + \frac{\partial}{\partial x_j}\left(\nu \frac{\partial \overline{u}_i}{\partial x_j} - \overline{u_i' u_j'}\right), \tag{2}$$

where $\overline{p}$ is the mean pressure, ρ the fluid density and ν the kinematic viscosity. Using the two-equation RANS approach, the Reynolds stresses ($\overline{u_i' u_j'}$) are prescribed in terms of the mean flow values, and the statistical turbulence closure (turbulence kinetic energy and turbulence dissipation rate equations) is based on the Boussinesq linear isotropic eddy-viscosity hypothesis, i.e. linear relationship between the turbulent stresses and the mean velocity gradients:

$$-\overline{u_i' u_j'} = 2\nu_t S_{ij} - \frac{2}{3}k\delta_{ij}, \tag{3}$$

where S_{ij} is the strain rate tensor, ν_t is the kinematic eddy viscosity, δ_{ij} the Kronecker Delta function and k is the turbulence kinetic energy (TKE). Buoyancy is usually not considered in urban wind energy applications, because a neutrally stratified atmospheric boundary layer is a common assumption, i.e. wind speed is strong enough for being considered as the predominant fluid flow factor (Tabrizi et al., 2014). The equations for TKE and the turbulence dissipation rate (ε) are necessary to solve all the unknowns (i.e. three components of averaged velocity, mean pressure, k and ε):

$$\frac{\partial\left(\overline{u}_j k\right)}{\partial x_j} = \frac{\partial}{\partial x_j}\left(\left(\nu + \frac{\nu_t}{\sigma_k}\right)\frac{\partial k}{\partial x_j}\right) + P_k - \varepsilon \tag{4}$$

and

$$\frac{\partial\left(\overline{u}_j \varepsilon\right)}{\partial x_j} = \frac{\partial}{\partial x_j}\left(\left(\nu + \frac{\nu_t}{\sigma_\varepsilon}\right)\frac{\partial \varepsilon}{\partial x_j}\right) + C_{\varepsilon 1}\frac{\varepsilon}{k}P_k - C_{\varepsilon 2}\frac{\varepsilon^2}{k}, \tag{5}$$

where $P_k = \nu_t S^2$ is the production of k, S is the modulus of the mean rate of strain tensor, and σ_k and σ_ε (Prandtl numbers), $C_{\varepsilon 1}$ and $C_{\varepsilon 2}$ are closure constants. The values of the constant parameters involved in RANS equations (i.e. closure constants, Prandtl numbers, von Kármán constant κ and proportional number C_μ) have a significant influence on simulation results near the roof surface. Toja-Silva et al. (2015a) carried out an extensive comparison of CFD simulation results using the standard values, the values proposed by Crespo et al. (1985) and those proposed by Bechmann and Sørensen (2010). Table 1 shows the standard values used for RANS equations constants, and those proposed by Crespo et al. (1985) and Bechmann and Sørensen (2010), respectively. Crespo et al. (1985) tailored the standard values using the atmospheric measurements of Panofsky and Dutton (1984), and Bechmann and Sørensen (2010) assumed a balance between viscous dissipation and shear production in the surface layer. Simulations that use the standard values show a worse agreement with wind tunnel experimental values for an isolated building. Being the hit rate (HR) the % of the simulation results that agree with a defined set of experimental data, a validation process is considered successful for values HR $\geq$ 66% (Santiago et al., 2007; Toja-Silva et al., 2015a). The highest hit rates (especially for TKE, the most complicated variable) were obtained using the values proposed by Bechmann and Sørensen (2010), but the best reproduction of the flow recirculation on the roof was obtained using the values proposed by Crespo et al. (1985). Both alternatives showed reasonably good results.

The production of TKE and the kinematic eddy viscosity

$$\nu_t = C_\mu \frac{k^2}{\varepsilon}, \tag{6}$$

are thermodynamic quantities involved in the RANS equations that are modelled using the standard $k-\varepsilon$ (SKE) turbulence model. Some modifications were introduced to the SKE model in order to improve the accuracy of the results, especially in order to reduce the overestimation of the TKE in the impinging region of bluff bodies. Such overestimation also leads to the underestimation (even to the non-reproduction) of the recirculation of the flow on the roof (Tominaga et al., 2008a; Shao et al., 2012; Toja-Silva et al., 2015a). Although the wake behind the building has less interest for urban wind energy application than the flow on the roof, it is important to mention that the most simple turbulence models also under-predict turbulence in the wake of bluff bodies. This is associated with the vortex formation and shedding behind the body and the often very high level of cross stream normal stress in comparison to the streamwise one.

Launder and Kato (1993) proposed to consider the vorticity scale (Ω) in the calculation of P_k (KL model), i.e.

$$P_k = \nu_t S \Omega. \tag{7}$$

However, the KL model has a mathematical inconsistency in the modelling of the Reynolds stresses and P_k. Additionally, the KL model

Table 1
Values used for RANS equations constants, in urban wind energy simulations.

Coefficients	C_μ	$C_{\varepsilon 1}$	$C_{\varepsilon 2}$	σ_k	σ_ε	κ
Standard coefficients	0.09	1.44	1.92	1.0	1.3	0.40
Crespo et al. (1985)	0.0333	1.176	1.92	1.0	1.3	0.42
Bechmann and Sørensen (2010)	0.03	1.21	1.92	1.0	1.3	0.40

overestimates P_k (compared with the SKE model) when Ω is higher than the strain rate scale. In order to correct these problems, Tsuchiya et al. (1997) introduced the Murakami-Mochida-Kondo (MMK) model that adds a modification to the expression for calculating ν_t only applicable when Ω is lower than the strain rate scale (the SKE expression for ν_t is applicable otherwise), i.e.

$$\nu_t = \frac{C_\mu k^2 \Omega}{\varepsilon S} \quad . \tag{8}$$

Durbin (1996) proposed another $k-\varepsilon$ modification in order to correct the TKE overestimation and the recirculation underestimation on the roof (stagnation point anomaly) in the SKE model. The stagnation point anomaly is addressed by relating ν_t to the turbulence velocity timescale (T), i.e.

$$\nu_t = C_\mu k\, T \, . \tag{9}$$

The Durbin model is based on the imposition of the "Realisability" constraint $2k \geq \overline{u_\alpha' u_\alpha'} \geq 0$ by bounding the turbulence velocity timescale as

$$T = \min(T_{SKE}, T_D) \, , \tag{10}$$

where $T_{SKE} = k/\varepsilon$ is the timescale computed according to the SKE turbulence model and

$$T_D = \frac{1}{3 C_\mu S} \sqrt{\frac{3}{2}} \tag{11}$$

is the bounded timescale proposed by Durbin (1996). The procedure leads to a reduction of the TKE overestimation at the impingement wall and to the more accurate reproduction of the recirculation flow on the building roof. However, although the overestimation is significantly reduced, it still remains. The recirculation length (X_R) is the distance of the flow recirculation on the roof normalized using the whole roof length. This model tends to overestimate X_R both on the roof and beyond the building. According to Durbin (1996), the constant parameter in the expression derived for computing T_D can be modified in order to obtain a better agreement with experimental data. Toja-Silva et al. (2015a) have empirically found that there exists a linear relationship between the constant parameter used in the definition of T_D and the recirculation length, as shown in Fig. 1. Toja-Silva et al. (2015a) found that the recirculation length of the flow on the roof can be exactly matched by relaxing the Realisability constraint proposed by Durbin (1996). The optimum constant factor for the calculation of T_D was determined carrying out a sensibility analysis. As shown in Fig. 1, other researchers (Tominaga et al., 2008a) have also relaxed this Realisability constraint.

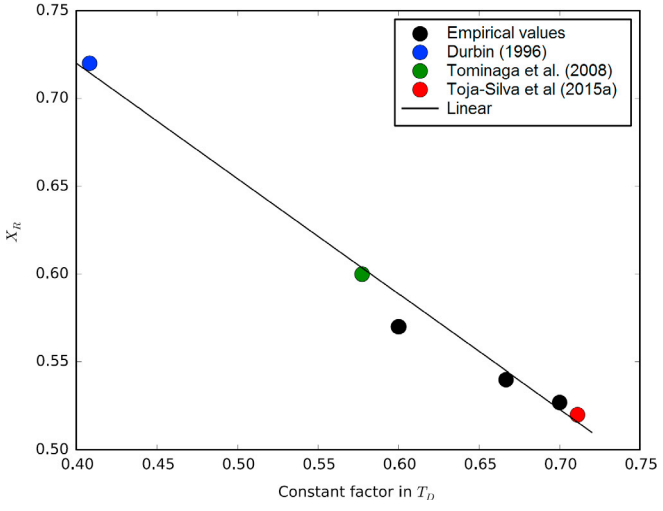

Fig. 1. Sensitivity analysis for the recirculation distance (X_R) of the flow on the building roof by varying the constant factor in the definition of the turbulence velocity time scale (T_D). Adapted from Toja-Silva et al. (2015a).

Yap (1987) also proposed a correction for the $k-\varepsilon$ model. It consists in the addition of a source term that depends on the normal distance to the nearest wall in the turbulence dissipation rate equation (Eq. [5]). Yap's correction is normally applied simultaneously with the KL model, yielding to the KLY model (Launder and Kato, 1993). Yakhot and Smith (1992) developed the $k-\varepsilon$ Re-Normalisation Group (RNG) model, also by adding a source term to the ε equation.

Nonlinear $k-\varepsilon$ RANS turbulence models were also used (Shao et al., 2012). The nonlinear eddy viscosity models have been developed to improve the Boussinesq approximation adopted in the linear eddy viscosity turbulence models keeping the stability and applicability conditions. Shih et al. (1993) presented a quadratic nonlinear eddy viscosity model by truncating the cubic and higher order terms in the general expression of the turbulent stresses, i.e.

$$-\overline{u_i' u_j'} = 2\nu_t S_{ij} - \frac{2}{3} k \delta_{ij} - C_1 \nu_t \frac{k}{\varepsilon} \left(S_{ik} S_{kj} - \frac{1}{3} S_{kl} S_{kl} \delta_{ij} \right) , \tag{12}$$

where C_1 is an empirical coefficient. Notice that the linear models (i.e. Eq. [3]) truncate quadratic and higher order terms. A quadratic eddy viscosity model allows the inclusion of the normal stress anisotropy. By considering the streamline curvature effects on the turbulent stresses, Craft et al. (1996) proposed a cubic eddy viscosity model that allows the successful inclusion of the normal stress anisotropy. Ehrhard and Moussiopoulos (2000) proposed another cubic eddy viscosity model with different constant values, to simulate the flow field around a cube in a channel. The computing time required for CFD simulations using nonlinear turbulence models is typically around 15% higher than using linear eddy-viscosity models (Ehrhard and Moussiopoulos, 2000).

In addition to the $k-\varepsilon$ turbulence models described previously, the $k-\omega$ shear stress transport (SST) was also used by some researchers for the CFD simulation of the wind flow around buildings. This model follows the $k-\omega$ approach at the near-wall region, and switches to the $k-\varepsilon$ away from the surface. The expression of the transport equation for k in the $k-\omega$ SST model is different from that in the $k-\varepsilon$ model (i.e. effective diffusivities are involved instead of viscosities), and a new equation for the specific dissipation (ω) is used (Menter, 1994), i.e.

$$\frac{\partial(\rho \overline{u}_j k)}{\partial x_j} = \frac{\partial}{\partial x_j} \left(\Gamma_k \frac{\partial k}{\partial x_j} \right) + \tilde{P}_k - Y_k \tag{13}$$

and

$$\frac{\partial(\rho \overline{u}_j \omega)}{\partial x_j} = \frac{\partial}{\partial x_j} \left(\Gamma_\omega \frac{\partial \omega}{\partial x_j} \right) + P_\omega - Y_\omega + D_\omega, \tag{14}$$

where, $\tilde{P}_k$ is the TKE generation due to the mean velocity gradients, P_ω is ω generation, Γ_k and Γ_ω, and Y_k and Y_ω are effective diffusivities and dissipations of k and ω, respectively, and D_ω is the cross-diffusion term.

Toja-Silva et al. (2015a) presented a rigorous validation of several RANS turbulence models (SKE, RNG, MMK, Durbin, Yap, Nonlinear Shih and $k-\omega$ SST) on an isolated building roof. The case study was the benchmark case A of the Architectural Institute of Japan (2017), with the experimental results of Meng and Hibi (1998). All the models tested successfully passed the validation threshold (hit rate above 66%) for velocity, but for the TKE only the RNG (with standard constants), MMK (with Crespo and Bechmann constants), all the Durbin variations (with Crespo and Bechmann constants, and the original Durbin model also with standard constants), Yap (with Bechmann constants) and Nonlinear Shih passed the validation. A very small recirculation of the flow was observed using the SKE model (specially using standard constants), and the recirculation exceeded the roof length using both Nonlinear Shih and $k-\omega$ SST models (notice that the recirculation distance is near the half

length of the roof in the experiment). The Durbin model variation proposed in Toja-Silva et al. (2015a) gave the best results (using Crespo constants) considering both hit rates and the recirculation of the flow, and the MMK model (with Crespo constants) gave the best hit rates and a reasonably good agreement with the recirculation of the flow in the experimental data. A very important observation is that the most difficult variable to simulate in urban environments (and in complex terrain in general) is TKE. Furthermore, since TKE is frequently used as a qualitative predictor of wind turbine damage, a very strong effort regarding this issue is necessary to ensure accurate CFD simulations.

Tominaga et al. (2008a) carried out a comparison between experimental and simulation results using some RANS turbulence models (SKE, KL, MMK and Durbin) for the wind flow around an isolated building (i.e. over the roof and also in the wake of the building). The SKE model did not reproduce the recirculation of the flow on the roof. The rest of the $k-\varepsilon$ models tested overestimated the reattachment length behind the building in comparison with the SKE model. The Durbin turbulence model showed the closest agreement with the experiment.

Shao et al. (2012) also carried out a comparison between experimental and simulation results for the same case study using nonlinear $k-\varepsilon$ turbulence models. They found that the steady calculation using the non-linear models cannot reach convergent solutions. The Craft model showed the best agreement regarding the reattachment length on the building roof, while the other non-linear models produced excessively large recirculation vortexes that extend over the entire roof without attachment. As stated above, this excessive recirculation was also obtained by Toja-Silva et al. (2015a) using the Shih model. All the nonlinear models compared in Shao et al. (2012) overestimated the reattachment length behind the building when compared with the wind tunnel experiment. The Craft model predicted the shortest reattachment length behind the building, yielding a value almost equal to the length given by the SKE model. The two other nonlinear models greatly overestimated the reattachment length by approximately three times the experimental value. On the building roof, the TKE predicted by the Ehrhard model agrees with the experimental data because the coefficients in that model were specifically calibrated for the wind flow over a cube. The two other nonlinear models in Shao et al. (2012) overestimated the TKE over the building roof, but such overestimation was smaller than that obtained using the SKE model. Behind the building, all the nonlinear models underestimated the TKE below the height of the building, especially both Shih and Ehrhard models. This TKE underestimation caused an overestimation of the reattachment length above the building roof when using these two nonlinear $k-\varepsilon$ models.

Yang et al. (2016) conducted CFD simulations of wind flow in a real urban area in Taipei (Taiwan). The wind speed, direction and turbulence intensity (TI) were compared with on-site measurement data to validate the computational model. The simulation results using the realizable $k-\varepsilon$ model yielded differences with the measurements for wind speed less than 10% in the windward region, and 20% in the leeward region. Wind direction matched well with measurements in general. According to Yang et al. (2016), the realizable $k-\varepsilon$ model provided more reasonable results for TI than those using SKE and RNG models, reaching a maximum difference with the experimental results of 16.5%.

2.1.2. Large-eddy simulation (LES)

Studies on urban wind energy using LES were conducted by Millward-Hopkins et al. (2012), Kono and Kogaki (2012) and Kono et al. (2016). In these studies, the governing equations were the filtered, incompressible continuity equation and the filtered, incompressible Navier-Stokes equations under neutral stability conditions:

$$\frac{\partial \overline{u}_i}{\partial x_i} = 0 \tag{15}$$

and

$$\frac{\partial \overline{u}_i}{\partial t} + \overline{u}_j \frac{\partial \overline{u}_i}{\partial x_j} = -\frac{1}{\rho}\frac{\partial \overline{p}}{\partial x_i} + \frac{\partial}{\partial x_j}\left(\nu \frac{\partial \overline{u}_i}{\partial x_j}\right) - \frac{\partial \tau_{ij}}{\partial x_j}, \tag{16}$$

where $\tau_{ij} = \overline{u_i u_j} - \overline{u}_i \overline{u}_j$ are the components of the subgrid-scale (SGS) stress tensor. For LES, the overbar denotes the filtering operator (overbar denotes averaged values for RANS). The filtering was implemented at the grid scale. The subgrid-scale (SGS) stresses were computed using the standard Smagorinsky model (Smagorinsky, 1991):

$$\tau_{ij} - \frac{1}{3}\tau_{kk}\delta_{ij} = -2\,\nu_{SGS}\,\overline{S}_{ij}, \tag{17}$$

where $\overline{S}_{ij}$ is the filtered rate of strain and $\nu_{SGS} = L_{SGS}^2 \overline{S}$ is the SGS turbulent viscosity, with $\overline{S}$ the characteristic filtered rate of strain, and L_{SGS} is the SGS mixing length computed as

$$L_{SGS} = \min\left(\kappa d, C_S V_c^{\frac{1}{3}}\right), \tag{18}$$

where d is the distance to the nearest wall, V_c is the volume of the computational cell and $C_S = 0.1$ is the Smagorinsky constant used or recommended by Rodi (1997), Murakami et al. (1999) and Sohankar et al. (1999) for flow past a rectangular cylinder or building. The optimal value of C_S varies from flow to flow and even point to point within one flow. In the near wall region, Kono and Kogaki (2012) and Kono et al. (2016) used Van Driest's damping function (Van-Driest, 1956) to meet the condition where the value of SGS stresses decreases drastically with a decrease in the distance from the nearest wall and becomes zero on the wall. Millward-Hopkins et al. (2012) used the Lilly's damping function that reduces the filter width within the viscosity-affected region so that the energy-carrying eddy sizes scale appropriately. To correct the drawback of a constant value of C_S, several models have been proposed. One of the well-known models is the dynamic Smagorinsky model proposed by Germano et al. (1991) and revised by Lilly (1992), which determines $(C_S)^2$ as a variable of space and time following the properties of the flow field, using two filters with different characteristics scales: a grid filter and a test filter. As compared to the standard Smagorinsky model, the accuracy of the dynamic Smagorinsky model for the flows around a square cylinder and around a wall-mounted cube is generally improved (Rodi, 1997; Murakami et al., 1999; Sohankar et al., 1999). However, the dynamic Smagorinsky model has a higher possibility of causing numerical instability (Ferziger and Peric, 2002).

Millward-Hopkins et al. (2012) investigated the validity of their LES approach by using the wind tunnel experimental results of flow over idealized urban pattern that were composed of rectangular blocks with heterogeneous height. Here, the wind tunnel experiment was conducted by Cheng and Castro (2002). The LES results of vertical profiles of mean wind speed above various blocks were matched well with the experimental data. However, the LES results of vertical profiles of streamwise and vertical turbulence generally underestimated the experimental data.

Kono and Kogaki (2012) and Kono et al. (2016) validated their LES approach using also the benchmark case A of the Architectural Institute of Japan (2017), which is a case study frequently cited in the literature for validation purposes, e.g. Toja-Silva et al. (2015a). The LES results of the streamwise, lateral and vertical components of mean velocity and TI around an isolated building matched well with the experimental data.

Tominaga et al. (2008a) carried out a comparison between experimental and simulation results using some RANS and LES turbulence models for the wind flow around an isolated building. Regarding LES, the standard Smagorinsky sub-grid model was used with the Smagorinsky constant $C_s = 0.12$. The overestimation of reattachment length behind the building obtained using RANS models was improved in the LES computations. This improvement is attributed to the better reproduction of the periodic velocity fluctuation due to the vortex shedding behind the building when using LES. The LES simulations in Tominaga et al. (2008a) were carried out with and without inflow turbulence. The LES without inflow turbulence produced too much vortex shedding behind the

building and, therefore, some discrepancies with the experimental results were observed, caused by the overestimation of velocity fluctuation in the lateral direction in the wake region. The result of LES with inflow turbulence showed a better agreement with the experiment concerning both velocity and TKE behind the building.

Gousseau et al. (2013) have also simulated the benchmark case A of the Architectural Institute of Japan (2017), and compared simulation results with the experiment of Meng and Hibi (1998). They carried out a rigorous validation and verification using LES turbulence modelling implemented in the commercial code ANSYS Fluent. They used the standard Smagorinsky model (testing the constant values $C_s = 0.1$ and $C_s = 0.15$) and its dynamic version. The use of $C_s = 0.1$ provided the most accurate results, very close to those of the dynamic Smagorinsky model. The vortex method to generate time-dependent velocity profiles at the inlet of the domain (inflow turbulence) showed to be suitable for atmospheric boundary layer flows. They obtained a very good agreement for mean streamwise velocity, but the validation was not successful for TKE. Thus, we can state that LES may be successfully validated for TKE focussing only on the roof, as Toja-Silva et al. (2015a) did using RANS.

2.1.3. Reynolds stress model (RSM)

The RSM (Launder et al., 1975) is a more elaborated turbulence model. Instead of assuming isotropic eddy viscosity, the RSM calculates the individual Reynolds stresses using differential transport equations together with an equation for the dissipation rate, i.e. 7 additional transport equations must be solved for three-dimensional flows.

Since the RSM takes into account the effects of streamline curvature, swirl, rotation and rapid changes in strain rate in a more rigorous manner than two-equation models (e.g. RANS), it may have a good potential for being used when the flow features of interest are the result of anisotropy in the Reynolds stresses, e.g. cyclone flows, highly swirling flows in combustors, rotating flow passages and stress-induced secondary flows in ducts.

The accuracy of RSM simulations is limited by the closure assumptions employed to model various terms in the exact transport equations for the Reynolds stresses. Additionally, the modelling of the pressure strain and dissipation rate terms is particularly challenging, and considered to be responsible for compromising the accuracy of RSM results. It is not yet demonstrated that the RSM yields clearly superior results than the other models, in order to justify the additional computational cost (ANSYS, 2017a).

Mertens et al. (2003) is the only study reported in the present review that used RSM for the CFD simulation of the urban atmospheric boundary layer. They commented on the theoretical advantage of the model, but they did not carry out a validation of the simulations by comparing with experimental data.

Mohamed et al. (2018) compared RANS and RSM simulations with new wind-tunnel measurements of all the terms involved in the TKE equation, for a two-dimensional stagnation flow around a flat plate. The SKE model over-predicted TKE, and Durbin's modified eddy viscosity reduced but did not avoid such over-prediction. Dissipation does not seem to be important in stagnation, and RSM models were not more accurate than two-equation RANS models. They showed that stagnation effects (large irrotational strain) cause not only a modification of the production term, but also affect advection and turbulent diffusion.

2.2. Numerical schemes

Although the use of 1st order (upwind) numerical schemes for the discretization of some convective terms is a common practice due to the highest stability of the algorithms, at least second order accurate numerical schemes (both central differencing and upwind) must be used for RANS in order to avoid problems with false diffusion (Rákai et al., 2014; Balogh et al., 2012; Bakker, 2016; Toja-Silva et al., 2015a). Fig. 2 shows a comparison of vertical profiles using RANS (Toja Silva et al., 2015a) for both streamwise velocity and TKE, for the wind flow around an isolated building using 1st and 2nd order numerical schemes for the discretization of the convective term of the momentum equation. The simulations with 2nd order schemes show a closer match to the experimental data for velocity and TKE. The improvement is clearly more significant for TKE.

With regard to discretization of the convection terms of the momentum equations for LES, it is ideal to use the second or higher order central differencing schemes in conjunction with sufficiently fine computational meshes so that the occurrence of severe numerical instability can be avoided, in particular, near the windward edge of a building. However, there are many cases where the use of such fine meshes is not possible. In these cases, it is recommended to blend a central differencing scheme and upwind schemes (Ono and Tamura, 2002). The relative weight for upwind schemes needs to be small enough to ensure that the flow field is not overly diffused and at the same time large enough to avoid the occurrence of severe numerical instability. Fig. 3 shows a comparison of vertical profiles, at the same location as in Fig. 2, of mean streamwise velocity and TKE using LES with upwind schemes or a blending scheme (Kono and Kogaki, 2012). The LES results with a blending scheme show a closer match to the experimental results for TKE, as compared to the LES with pure upwind schemes.

2.3. Meshing

The quality of the simulation results is conditioned by the mesh used, i.e. size and form of the grid. A high-quality body-fitted grid should avoid unstructured grids constituted by pyramidal and tetrahedral cells that

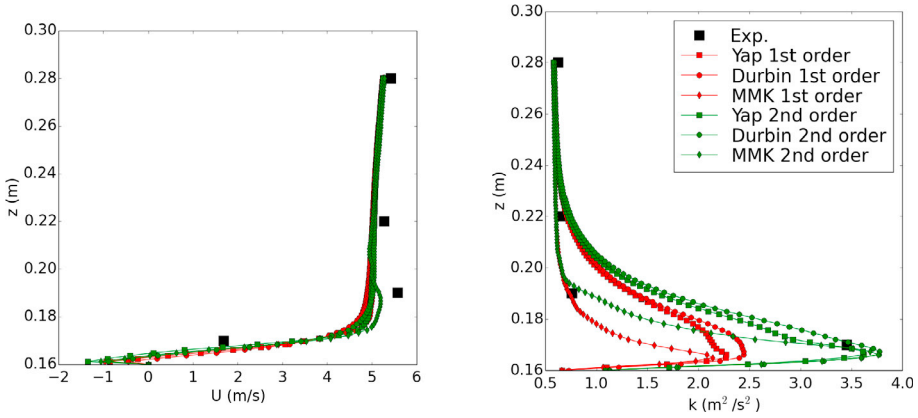

Fig. 2. Comparison of the vertical profiles using 1st and 2nd order numerical schemes for the discretization of the convective term of the momentum equation for the RANS turbulence modelling. This comparison corresponds to the vertical profile V3 (flow-recirculation region on the roof) in Toja-Silva et al. (2015a). Left: comparison of velocity. Right: comparison of turbulence kinetic energy. Note that z is the height from the ground.

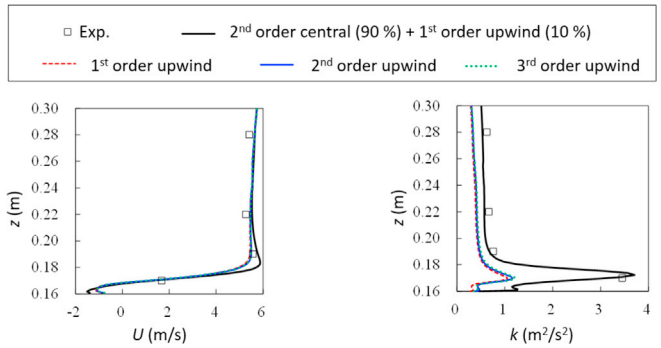

Fig. 3. Comparison of the vertical profiles of streamwise velocity and TKE obtained by LESs with discretization of the convection terms of momentum equations using upwind schemes (first order, second order, or third order), or a blending scheme of 90% of second order central differencing scheme and 10% of first order upwind scheme. The profiles of the blending scheme are from Kono and Kogaki (2012). The location of the vertical profiles corresponds to the vertical profile V3 (flow-recirculation region on the roof) in Toja-Silva et al. (2015a). Left: streamwise velocity. Right: turbulence kinetic energy.

can lead to problems for convergence when using high-order discretization schemes, decreasing the computational accuracy (Blocken et al., 2012). It is recommended to avoid extreme distortion of cells (e.g. angles $>90^{\circ}$ for triangles), especially in areas of large flow gradients. Near the walls it is preferably the use of parallel/perpendicular cells, i.e. quadrilateral, hexahedral or prism/wedge cells (van Hooff and Blocken, 2010).

The mesh resolution should be higher in regions where large flow gradients are expected, it means the application of a refinement in regions of interest. The discretization error must go to zero as the grid size tends to zero. The rate at which it takes place is given by the order of the numerical discretization. The Grid Convergence Index (GCI) can be computed by comparing the results obtained using different grid sizes, in order to quantify the discretization error in a CFD simulation (Roache, 1998; Hirsch, 2007; Ferziger and Peric, 2002). According to the Richardson extrapolation (Richardson, 1911), the mesh should be systematically refined or coarsened by a constant factor (typically 2 or $\sqrt{2}$). This is called solution verification, and has the goal of verifying that a grid-independent solution was obtained in the simulations.

All of the published CFD papers should show a solution verification process. However, only few works go beyond showing a convergence plot (comparing measurements with simulation results obtained using different grid sizes), and carry out a rigorous study involving calculation of GCI, e.g. Toja-Silva et al. (2015a) and Wang et al. (2018) with RANS and Gousseau et al. (2013) with LES. Using LES with implicit filtering, the model strongly depends on the grid size and, when refining the grid, the model contribution changes and a grid-independent solution cannot be found. Due to that, Gousseau et al. (2013) obtained a better agreement with experimental data on the coarsest computational grid, while a finer grid overestimated the TKE.

2.4. Best practice guidelines

Franke et al. (2007) presented a bestpractice guideline for the CFD simulation of flows in the urban environment, developed within the framework of the COST Action 732. The main objective of this action was to improve and to assure the quality of micro-scale meteorological models that are applied for predicting wind flow and transport processes in urban or industrial environments. These guidelines can be considered as a reference for urban wind CFD simulations still today, as they are followed by almost all the research articles related to this topic. It discussed very relevant aspects of atmospheric CFD simulations of urban areas that must be respected, e.g. domain dimensions, boundary conditions, meshing. As an extension, Tominaga et al. (2008b) further discussed the same aspects when the area of interest is at the pedestrian level (near the ground).

3. Building aerodynamics applied to the wind energy exploitation

The work of Mertens (2006) is the first significant study of building aerodynamics applied to the wind energy exploitation. He investigated the concentration effect of the wind on the roof, at building sides, between two airfoil-shaped buildings and in ducts through buildings. However, this investigation only used CFD for basic cases (e.g. flow around a flat plate, boundary layer, wind turbine blade in 2D), but not for the wind flow around buildings, where the flow velocity was computed using the potential theory (Batchelor, 1988). Mertens (2006) identified the interest of installing wind turbines in ducts through buildings in order to get the most of the pressure difference between up and downstream walls; however, that application was not extensively developed further. Concerning building roofs, Mertens (2006) mentioned that a sphere-like building was the most promising shape, estimating the energy concentration factor as 3 to 4 by using only the potential theory for computing velocity distribution around a sphere. This value is in a reasonably good agreement with that obtained by Toja-Silva et al. (2016) for an isolated building, who carried out a more sophisticated CFD investigation.

Apart from some isolated studies that will be commented later, the first exhaustive analysis of the most appropriate building shape for the wind energy exploitation on building roofs using CFD was done by Abohela (2012), who studied simple geometric roof shapes: flat, domed, gabled, pyramidal, barrel vaulted and wedged. Afterwards, Toja Silva (2015) focussed on building-roof shape (empirical) optimization for urban wind energy, carrying out CFD simulations of more complex shapes, including several additional aspects such as wall-roof coupling, compatibility between solar and wind energies and the effect of the roof-edge shape, building aspect ratio and surrounding buildings on the wind flow. An exhaustive validation and customization of RANS turbulence models for urban wind simulations was also presented. Details of these investigations are explained below.

Table 2 shows a summary of the specific investigations cited in the present review. The majority of investigations were carried out using steady RANS turbulence models (66%), followed by unsteady RANS (URANS), being 21% of the cases. Only 10% of the articles cited were conducted using LES, and only Mertens et al. (2003) used RSM. Regarding the software, 62% of the reported investigations used the commercial code ANSYS (2017b), including both CFX and Fluent, more than 20% used the free and open source software OpenFOAM (2017), 7% used the Japanese code FrontFlow/red (Center for Research on Innovative Simulation Software, 2017), and EllipSys (Sørensen, 1995), WindSim (2017) and STAR-CD (Siemens, 2017) were used in only 1 of the reported works, respectively. More than half of the investigations reported (57%) studied an isolated building, including Nuland (2017) that simulated a farm fish barge, and Lu and Ip (2009) and Wang et al. (2015) that studied groups of 1–3 and 2 isolated buildings, respectively. Analyses of simplified urban patterns and studies of a target building with simplified surrounding were conducted in near 29% of the cases reported. The works that deal with a real urban area only represent the 14% of the total. Regarding the scale of the geometry, 70% of the cases conducted full scale simulations, what is one of the clear advantages of the CFD (numerical experiments) in front of experimental measurements. The 27% of the investigations used wind-tunnel scale buildings, normally adapting the same geometry of models used for validation purposes. The rest corresponds to Aquino et al. (2017) that used a reduced-scale model, but higher than wind-tunnel (with few meters of order of magnitude) because they add wind belts (with very small dimensions) to the building. The most important features of each investigation are commented in Sections 3 and 4. The statistics discussed above are presented in a visual way in Fig. 4.

Table 2
Summary of the state-of-the-art.

Article/Ph.D. Thesis	Turbulence modelling	Software	Urban environment type	Scale	Important features
Abohela (2012) Abohela et al. (2013)	RANS	ANSYS	Target building with simplified urban surrounding	Wind tunnel	Best basic building-roof shape for wind energy: vaulted roof. Influence of building height and incident wind direction.
Aquino et al. (2017)	RANS	ANSYS	Isolated building	Reduced scale	Passive integration of aero-elastic belts (wind belts). Siting and power assessment.
Beller (2011)	RANS	EllipSys	Simplified urban pattern	Full scale	Discussion of TKE and wind power potential for simplified city patterns. Wind turbines positioning for particular cases.
Hassanli et al. (2017)	RANS URANS	ANSYS	Isolated building	Wind tunnel	Double-skin façade system. Wind turbines positioning assessment.
Heath et al. (2007)	URANS	ANSYS	Simplified urban pattern	Full scale	Wind turbines positioning on pitched roof, attending only to velocity. Example of energy yield facility in London.
Kono and Kogaki (2012)	LES	FrontFlow/red	Isolated building	Wind tunnel	Study of wind power density and velocity standard deviation at different heights above the roof.
Kono et al. (2016)	LES	FrontFlow/red	Isolated building	Wind tunnel	Wind turbine positioning for different incident wind directions on flat-roof buildings with different horizontal aspect ratios.
Krishnan and Paraschivoiu (2016)	URANS	ANSYS	Isolated building	Full scale	Simulation of a real Savonius (VAWT) in horizontal position on a building roof, including a diffuser around the turbine: power coefficient of the turbine is improved from 0.135 to 0.34 due to the diffuser.
Larin et al. (2016)	URANS	ANSYS	Isolated building	Full scale	Simulation of a real Savonius (VAWT) in horizontal position on a building roof. Demonstration of the importance of simulating both building and wind turbine to asses a correct performance. Wind turbine geometry optimization for the wind flow on the roof: power coefficient 5–10 times higher than in open field.
Ledo et al. (2011)	RANS	ANSYS	Simplified urban pattern	Full scale	Comparison among flat, pitched and pyramidal roofs: higher available power on flat roof.
Liu et al. (2017)	RANS	ANSYS	Real urban area	Full scale	Validation using measurements on the site. Scaling issues between full-scale and wind-tunnel simulations due to the consideration or not of the surrounding buildings in the simulations.
Lu and Ip (2009)	RANS	ANSYS	1-3 isolated buildings	Full scale	Comparison of flat and shed roofs attending to both wind velocity and TKE: flat roof resulted better.
Millward-Hopkins et al. (2012)	LES	ANSYS STAR-CD	Simplified urban pattern	Wind tunnel	Use the CFD simulations produced by Xie et al. (2008). Wind turbine positioning on building roof surrounded by urban pattern. Quantification of uncertainties accumulated errors in final wind speed predictions on building roofs.
Mertens et al. (2003)	RSM	ANSYS	Isolated building	Full scale	Simulation of a Darrieus (VAWT) on a building roof using actuator disc model. Analysis of wind conditions on the roof and turbine location as function of energy yield.
Micallef et al. (2016)	RANS	ANSYS	Isolated building	Full scale	Simulation of a HAWT on a building roof using actuator disc model. Analysis of wind turbine effect: strong influence on the flow observed.
Nuland (2017)	RANS	OpenFOAM	Isolated (fish farm barge)	Full scale	Simulation of HAWT and VAWT on a fish farm barge using actuator line model.
Simões and Estanqueiro (2016)	RANS	WindSim	Real urban area	Full scale	Wind speed and power density assessment on buildings roofs in Cascais, Portugal. Comparison with experimental measurements at site.
Tabrizi et al. (2014)	RANS	ANSYS	Real urban area	Full scale	Study of an industrial building: large-surface low-rise. Comparison with velocity measurements on the site. Sitting of HAWT attending to the wind horizontality: centre of the roof.
Toja-Silva et al. (2013)	URANS	ANSYS	Isolated building	Full scale	Qualitative assessment of the effect on wind turbines of the urban wind variability.
Toja Silva (2015)	RANS	OpenFOAM	Target building with simplified urban surrounding	Wind tunnel and full scale	Validation of several RANS turbulence models. Wind turbines positioning according to TI. Compatibility between wind and solar energies on a building roof. Effect of roof-edges on the wind flow. Optimum building-roof shape for wind energy: spherical roof coupled with a cylindrical wall. Influence of the building aspect ratio and surrounding buildings height.
Toja-Silva et al. (2015a)	RANS	OpenFOAM	Isolated building	Wind tunnel	Validation of different RANS turbulence models. Effect of different constants in Navier-Stokes equations. Wind turbines positioning according to TI.
Toja-Silva et al. (2015b)	RANS	OpenFOAM	Isolated building	Wind tunnel and full scale	Effect of roof-mounted solar panels on the wind flow: slightly increasing speed and decreasing TI. Wind turbines positioning according to velocity and TI. Scaling issues reported between wind-tunnel and full scale simulations due to similitude constraints (i.e. different Re number).
Toja-Silva et al. (2015c)	RANS	OpenFOAM	Isolated building	Full scale	Analysis of state-of-the-art roof shapes: spherical roof showed promising attending to velocity and TI. Effect of the roof edge shape on the wind flow.

(*continued on next page*)

Table 2 (*continued*)

Article/Ph.D. Thesis	Turbulence modelling	Software	Urban environment type	Scale	Important features
Toja-Silva et al. (2016)	RANS	OpenFOAM	Target building with simplified urban surrounding	Full scale	Empirical-heuristic optimization of building-roof shape for wind energy. Optimum shape: exact spherical roof coupled with a cylindrical wall. Influence of the building aspect ratio and surrounding buildings height. Estimation of power increase on the roof due to the optimum shape: up to 3 times the open field power. Example of wind turbines installation: around 20 kW instantaneous power.
Wang et al. (2015)	RANS	ANSYS	Two isolated buildings	Full scale	Study of the Venturi effect in urban environments (buildings in converging and diverging positions).
Wang et al. (2018)	RANS	ANSYS	Isolated building	Full scale	Use of semi-log wind profile to predict the canopy velocity. Validation using wind Lidar measurements on a real building roof. Wind turbines positioning according to velocity and TI.
Yang et al. (2016)	RANS	ANSYS	Real urban area	Full scale	Validation of CFD simulation results of a real urban area by comparing with measurements on the site for both wind speed and TI. Study of wind turbines positioning according to wind speed and turbulence intensity: windward side of the roof showed advantageous. Analysis of roof variations: curved edge led to lower TI and higher velocity.
Zanforlin and Letizia (2015)	URANS	ANSYS	Target building with simplified urban surrounding	Full scale	Simulation (in 2D) of a real Darrieus (VAWT) installed in horizontal position on a pitched roof. Demonstration of the importance of simulating both building and wind turbine with the diffuser to asses a correct performance. Effect of integration of rooftop and diffuser: power increase for skewed winds and abatement of torque fluctuations.

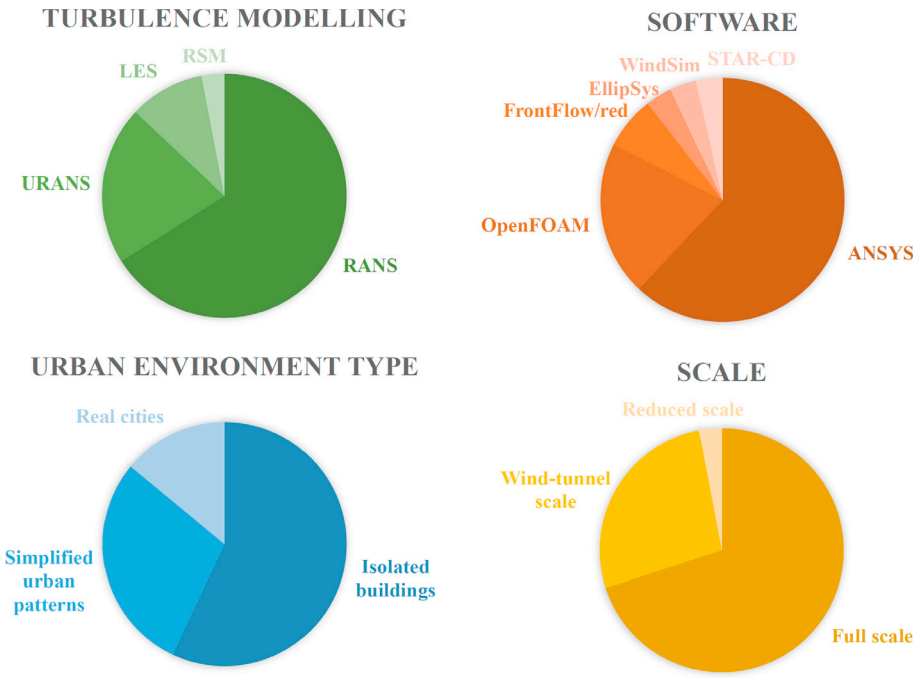

Fig. 4. Statistics of the state-of-the-art investigations.

3.1. The isolated building

Lu and Ip (2009) presented a study of the urban wind power feasibility in Hong Kong. This work can be considered as one of the pioneer in this matter. They stated the necessity of using CFD for modeling annual wind flows over particular buildings, in order to assess the wind power and to analyze wind turbines location on the roof considering both wind speed and TKE. They recommended to "avoid the turbulence layer" when installing a wind turbine; this concept was developed further by Toja-Silva et al. (2015a) by introducing the TI threshold for horizontal axis wind turbines (HAWT) as TI = 0.15. According to Lu and Ip (2009), the flat roof shape was the optimal (comparing only with shed roof) for the wind energy exploitation attending to both wind velocity and TKE. They reported a concentration effect on the wind that could increase the wind power density (wind power per unit of swept surface) by a factor of 3–8. They simulated the wind flow around an isolated building, and a series of 2 and 3 buildings. The SKE turbulence model was used in ANSYS Fluent.

Kono and Kogaki (2012) investigated the wind conditions over a flat-roof building for installing wind turbines. Their LES simulations (standard Smagorinsky with $C_s = 0.1$) used the software FrontFlow/red to study the benchmark case A of the Architectural Institute of Japan (2017). They computed the wind power density and plotted velocity standard deviation at different heights above the roof, yielding higher wind power densities and lower velocity standard deviations around the

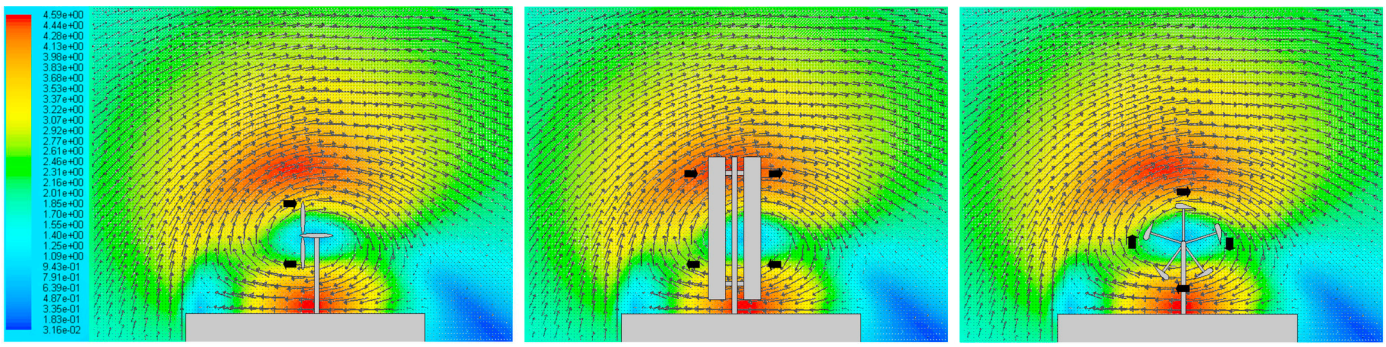

Fig. 5. Superimposition of HAWT (left), VAWT (centre) and VAWT in horizontal position (right) over the wind flow on a flat-roof building. It is observed that the HAWT cannot work under these conditions, the VAWT can work, and the VAWT in horizontal position takes a great advantage of the flow conditions. Adapted from Toja Silva (2015).

upstream edge of the roof. They found several regions on the roof with values of standard deviation that exceeded the maximum streamwise wind velocity component recommended by the normative IEC61400-2 (International Electrotechnical Commission, 2006) for conventional wind turbines. Standard deviations of streamwise velocity were found much larger than those of spanwise and vertical velocities, except near the roof surface. Although TKE is frequently used as a qualitative predictor of wind turbine damage, a rigorous fatigue indicator requires the determination of the frequency. Since TKE is broadband, LES shows a great potential because of its ability to detect important frequencies such as building vortex shedding frequency, in spite of its higher computational cost.

Toja-Silva et al. (2013) conducted CFD simulations of the wind flow around a simple building to qualitatively assess the effect of the highly variable wind conditions over a building roof on wind turbines. URANS turbulence modelling was used in the software ANSYS. As shown in Fig. 5, the sections of various types of wind turbines were superimposed over the velocity field obtained from the simulations, and their aerodynamic behaviour was analysed in a qualitative manner. Horizontal-axis wind turbines (HAWT) showed higher performance in flat terrain applications or on large structures, whereas in urban environments the higher potential of vertical-axis wind turbines (VAWT) was demonstrated. Further descriptions of HAWT and VAWT conventional and non-conventional models can be found in Eriksson et al. (2008), Ishugah et al. (2014) and Murthy and Rahi (2017).

Abohela et al. (2013) performed CFD simulations with the purpose of identifying the effect of different roof shapes on the generated energy. As shown in Fig. 6, the roof shapes were flat, domed, gabled, pyramidal, barrel vaulted and wedged. The highest speed-up was found for the vaulted roof, with an increase in the generated electricity up to 56.1%. The realizable $k-\varepsilon$ RANS turbulence model implemented in ANSYS Fluent was used for the simulations. The effect of a general pattern of surrounding buildings was studied, as well as different incident wind directions. For all the shapes tested, the region of maximum TI was identified over the roof below $z/H = 1.3$, where z is the height above the ground and H the building height (note that $z/H = 1.0$ corresponds to the roof surface), hence wind turbines were recommended to be installed above this threshold. This threshold height is in agreement with Toja-Silva et al. (2015a) for a flat roof, but a more detailed study of Toja-Silva et al. (2015c) found different threshold heights for different roof shapes, assuming TI = 0.15 as the threshold for installing HAWT. According to Toja-Silva et al. (2015a-c, 2016), VAWT can be installed below such threshold height. Toja-Silva et al. (2016) found also a variation of this threshold height depending on the surrounding buildings.

Toja-Silva et al. (2015a) proposed a method for wind turbines positioning on building roofs according to TI. They defined with a general rule for HAWT positioning, i.e. above $z/H = 1.31$. This height was obtained by analysing the fluid field on the roof, considering TI = 0.15 as the threshold for installing a HAWT due to safety and durability reasons, according to the European Wind Turbine Standards II (Pierik et al., 1999). As shown in Fig. 7, a detailed study for different roof regions is presented in Toja-Silva et al. (2015a). The authors also studied different incident wind directions, yielding lower threshold heights than for an incident wind normal to the building wall. Below this threshold height, other wind turbine configurations may be considered, e.g. new concept, vertical axis wind turbines (VAWT). Additionally, the installation of a VAWT in horizontal position near the upstream edge of the roof is proposed as an interesting application for taking the most of the recirculation of the flow in this roof region.

As mentioned before, major barriers for urban wind energy are disadvantages in front of other simpler and more robust technologies, i.e. photovoltaics. Since the latest technology developments in hybrid renewable energy systems allow, by combining different renewable sources, to obtain efficiencies higher than that obtained from single

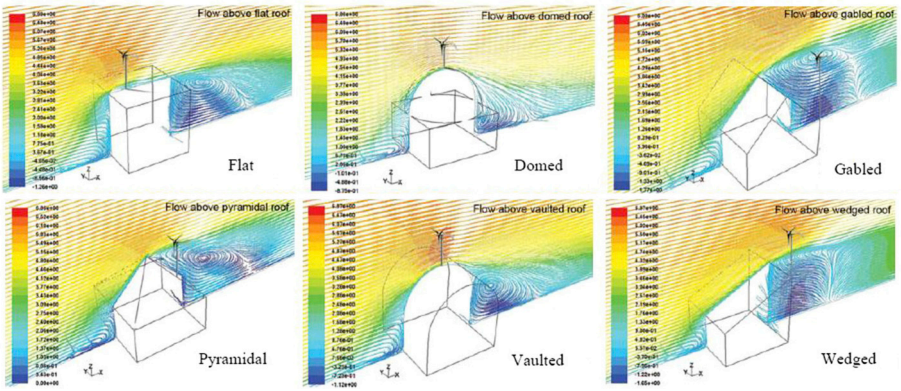

Fig. 6. Optimum location for installing a HAWT on different roof shapes. (Abohela et al., 2013).

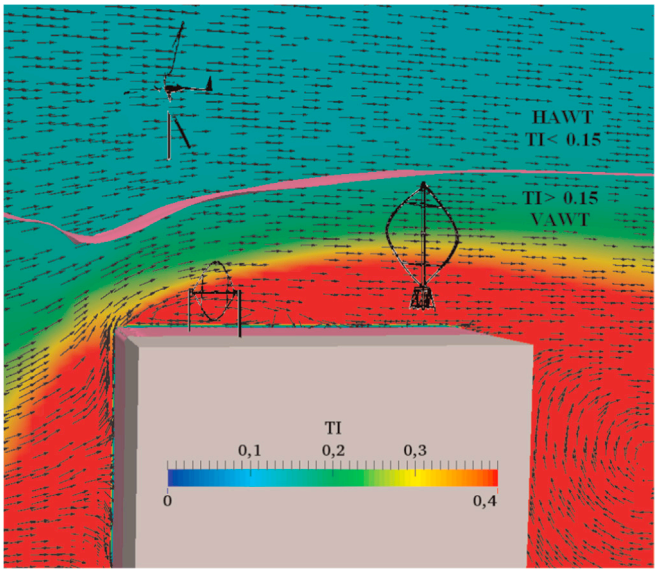

Fig. 7. Wind turbine positioning according to the turbulence intensity. The vector field is velocity, the background colormap corresponds to the turbulence intensity (TI) and the bold line (in magenta) is an isocontour for TI = 0.15 (Toja-Silva et al., 2015a).

power sources (Khare et al., 2016), it is important to demonstrate the compatibility between solar and wind energies on buildings roofs in order to clarify that such technologies are not competitors but collaborators. In this regard, Toja-Silva et al. (2015b) presented an investigation of the effect of roof-mounted solar panels on the wind flow from the point of view of the wind energy exploitation. CFD simulations were performed using a customized Durbin RANS turbulence model implemented in OpenFOAM. The wind flow on an empty roof was compared with roof-mounted solar panels with different tilt angles. No significant differences compared to the empty roof were found above the isoline of TI = 0.15. Below this isoline, mean wind velocity slightly increased and TKE significantly decreased due to the presence of the solar panels. The decrease of the TKE was attributed to the damping effect of recirculation vortices appearing between the solar arrays (Toja-Silva et al., 2015b), shown in Fig. 8 (left). The wind flow was analyzed and the most adequate wind turbine model for each roof region was suggested. Additionally, full-scale building simulations were compared with reduced-scale model, and scaling issues were reported. As shown in Fig. 8 (right), a massive recirculation takes place for this specific case due to the interaction of the neighboring vortices between the arrays. This massive recirculation was not identified at a reduced-scale model. There is a difference of 2 orders of magnitude in the Reynolds number. Since the Reynolds number for the wind tunnel case is much lower, the fluid flow becomes laminar between the solar panels and the roof surface. Such scaling issue shows the necessity of simulations and experimental studies considering full-scale conditions, especially when dealing with small openings.

Toja-Silva et al. (2015c) continued the study of Toja-Silva et al. (2015a) and Abohela et al. (2013) by simulating the wind flow around the state-of-the-art roof shapes (i.e. common roof shapes in the literature, e.g. in Fig. 6). Vertical profiles of velocity, TKE and TI were compared. The TI threshold for HAWT was also compared for the state-of-the-art roof shapes. The results showed a similar flow behavior on the sharp (pitched and shed) and on the curved roofs (spherical and vaulted), respectively. A higher velocity was observed on the curved shapes (spherical and vaulted). Non horizontal velocity was observed on the sharp roofs (flat, pitched and shed). Much lower TI values were found for the curved shapes, especially for spherical shapes. Among the state-of-the-art geometric shapes, spherical and vaulted roofs were the best options found for the wind energy exploitation. Toja-Silva et al. (2015c) also analyzed the influence of the roof edge shape on the wind flow. The results showed a similar behavior of the flow over the simple edge and the cantilever edge. A massive recirculation of the flow that exceeded the roof length was observed for the railing edge, and the height of the TI threshold increased. A very small recirculation was observed for the curved edge case, speed-up was reported around the upstream edge, and the TI threshold height substantially decreased. The transition between walls and roof showed a strong influence on the behavior of the flow.

Kono et al. (2016) analyzed the effect of the incident wind direction for installing wind turbines on flat-roof buildings with different horizontal aspect ratio. This work is an extension of the previous study of Kono and Kogaki (2012). The standard Smagorinsky LES model was also used implemented in the CFD software FrontFlow/red. As shown in Fig. 9, results showed that wind velocity tends to decrease as the building width decreases. The upstream corners of the roof showed the most favorable conditions for a wind turbine at low heights. Downstream locations showed worse performance at lower heights due to a much higher turbulence intensity, as shown in Fig. 9 (right). Thus, wind turbine installation may be recommended at higher heights. When there is no prevailing wind direction, the authors recommended installing a wind turbine on the center of the roof, but high enough for avoiding the high turbulence region.

Toja-Silva et al. (2016) carried out an empirical-heuristic

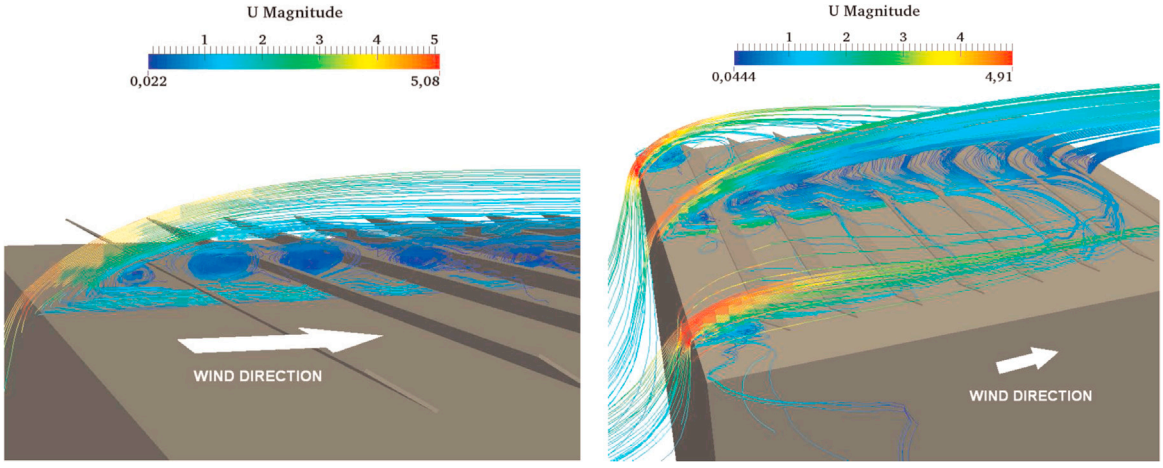

Fig. 8. Effect of solar panels on the wind flow: streamlines that show the recirculation vortices on the roof (left), and massive recirculation observed for the same particular case in a full-scale simulation (right) (Toja-Silva et al., 2015b).

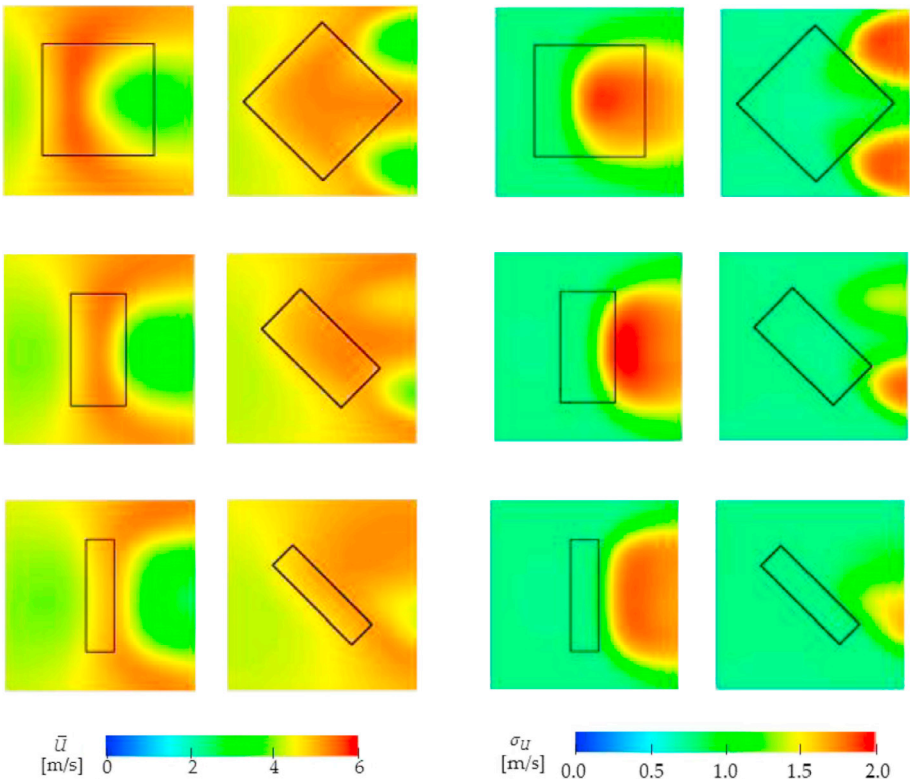

Fig. 9. Horizontal distribution (at $z/H = 1.15$) of mean wind speed (left) and standard deviation of horizontal velocity, σ_U (right); for different horizontal aspect ratios. Adapted from Kono et al. (2016).

optimization of the building-roof shape. Such optimization started from the spherical roof reported in Toja-Silva et al. (2015c), and added an analysis of the roof-wall transition geometry by testing different variations of a spherical roof, a roof-width sensitivity analysis of the optimum geometry and an exploration of the building aspect ratio effect on the flow. Velocity, TKE and TI were compared and the wind turbine positioning on the roof was analyzed in detail. An exactly spherical roof coupled with a cylindrical wall was identified as the optimum shape for the wind energy exploitation. For this shape, as shown in Fig. 10, the speed-up was the highest among the alternatives compared, not only on the top of the roof but also on the upper area of the walls, and the TI threshold was not reached for the isolated building (height of the threshold = 1.0). Thus, a HAWT can be installed on the roof at any height. An additional advantage of the spherical roof with a cylindrical wall is that the flow behavior is the same for all the incident wind directions. It is also observed in Fig. 10 that the vaulted roof has the highest TI threshold height and the speed-up is only higher than the spherical roof tested by Abohela et al. (2013), but lower than the other alternatives, especially lower than the optimum building-roof shape. The roof-width sensitivity analysis revealed that the exact sphere is the most advantageous shape attending to both speed-up and TI. Regarding the aspect ratio, slender shapes showed higher speed-up and lower TI values.

Hassanli et al. (2017) simulated a double-skin façade system with strategic openings, from the point of view of the wind energy exploitation. They compared the results obtained using the $k-\omega$ SST RANS turbulence model with the unsteady scale adaptive simulation (SST-SAS) model, which solves the turbulence length-scales on a fine enough mesh and defaults to URANS in regions where the mesh is coarser. ANSYS Fluent was used for the simulations. The results were compared with wind-tunnel measurements of mean speed, yielding a reasonably good accuracy (inside a range of 15%). Additionally, small differences were found between the results using URANS and RANS. Fig. 11 shows the mean speed distribution inside the cavity. Different incident wind directions were analysed. The flow became more

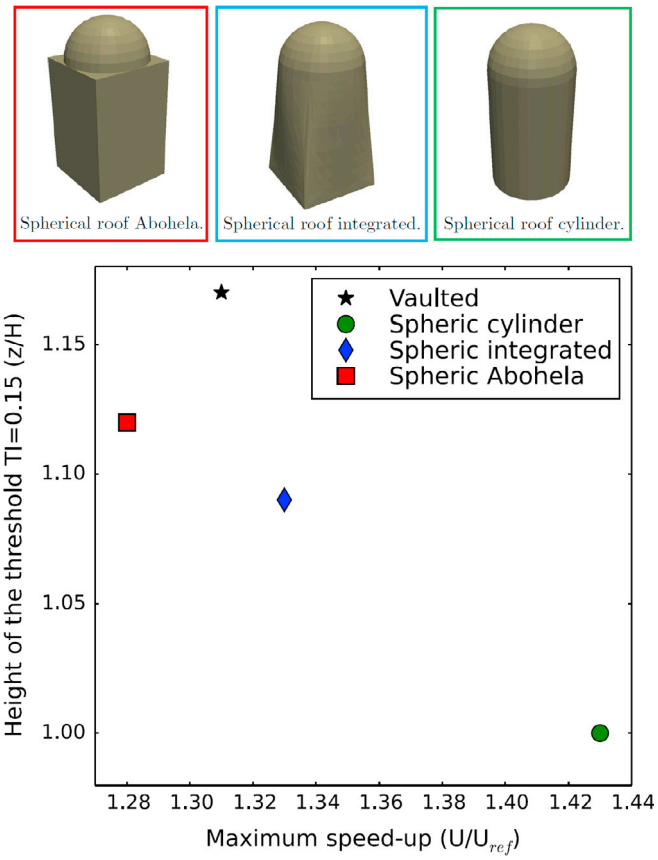

Fig. 10. Optimum building-roof shape: TI threshold height vs. speed-up for different alternatives. Adapted from Toja-Silva et al. (2016).

uniform and the turbulence progressively decayed as flow progressed through the cavity. The regions in the middle of both the leading and trailing sides of the cavity were considered favourable locations for installing wind turbines, where high velocity, uniform flow and low turbulence were observed. The double-skin façade system with strategic opening not only dissipated the turbulence created by the sharp corners, but also contributed to the dissipation of the turbulence existing in the free stream flow.

Wang et al. (2018) performed CFD simulations of wind flow above an isolated low-rise building. Although it has the plant of a real building (Engineering and Technology Building, Inner Mongolia University of Technology, China), it can be considered as flat-roof near--rectangular (60 × 100m plant and 20m high). They used the realizable $k-\varepsilon$ RANS turbulence model in the commercial software ANSYS Fluent. Although they did not consider surrounding buildings, they utilized a semi-log wind profile in order to predict the canopy velocity. Such semi-log profile describes the velocity with a logarithmic wind profile above the building height and an exponential wind profile below it. The simulations were successfully validated by comparing wind velocity and turbulence intensity with wind Lidar measurements. The grid convergence index was calculated in order to verify the solution. They used the simulation results for wind turbines sitting on the roof, avoiding high turbulence intensity regions and searching the maximum wind-accelerating factor. They propose optimum mounting locations and installation heights for wind turbines. They have considered TI = 0.25 as the maximum admissible value for wind turbines, according to the IEC Standard 61400-2 (International Electrotechnical Commission, 2006). Such normative is less restrictive than the European Wind Turbine Standards II (Pierik et al., 1999), used in other investigations (e.g. Toja-Silva et al., 2015a), that mention TI = 0.15 as the threshold value for installing a HAWT due to safety and durability reasons. However, Wang et al. (2018) obtained a threshold height in agreement with Toja-Silva et al. (2015a), i.e. $z/H = 1.30 \sim 1.50$ for the annual averaged wind speed in the prevailing wind direction. The best locations are also found at the upstream edge of the roof.

3.2. The influence of surrounding buildings (urban environment)

Heath et al. (2007) carried out CFD simulations of the wind flow around an array of pitched-roof buildings, studying different incident directions. The SKE URANS turbulence model implemented into the software ANSYS CFX was used for the simulations. They only focus on velocity, neglecting the effect of TKE. They state that the speed-up effect observed above the top of the roof is not present when the building is immersed in an urban environment. A strong effect of the incident wind direction is reported, and they discuss the most recommended site for installing wind turbines for different incident directions. They discuss the energy yield for a hypothetical facility in London, considering the local regulations and yearly-averaged wind conditions.

Beller (2011) presents CFD simulations of the wind flow around a general urban pattern, and a discussion about the TKE and the wind power potential obtained in such environments. The SKE RANS turbulence model was used, implemented into the software EllipSys. Wind turbines positioning for particular case studied are presented, and the interest of installing VAWT in horizontal position close to the upstream edge is commented.

Ledo et al. (2011) simulated the wind flow around three suburban landscapes (matrix of 3 × 3 buildings): pitched, pyramidal and flat roofs. The steady state $k-\omega$ SST RANS turbulence model is used for the simulations, with the software ANSYS CFX. Wind turbine positioning is discussed for each roof type. They obtained lower TI and considerably higher velocity on the flat roof compared to the other shapes tested. The wind power density above flat roof was also found greater and more consistent (i.e. less dependent on wind conditions, especially direction) than above the other roof types, independently of the incident wind direction.

Millward-Hopkins et al. (2012) investigated the wind flow over a simplified urban pattern, in order to make suggestions for ideal rooftop turbine locations. They suggest the upstream edge of the roof as the most adequate position, although they comment that the turbine can be installed behind this edge at higher heights, having then the advantage of increasing the available resource from non-prevailing wind directions.

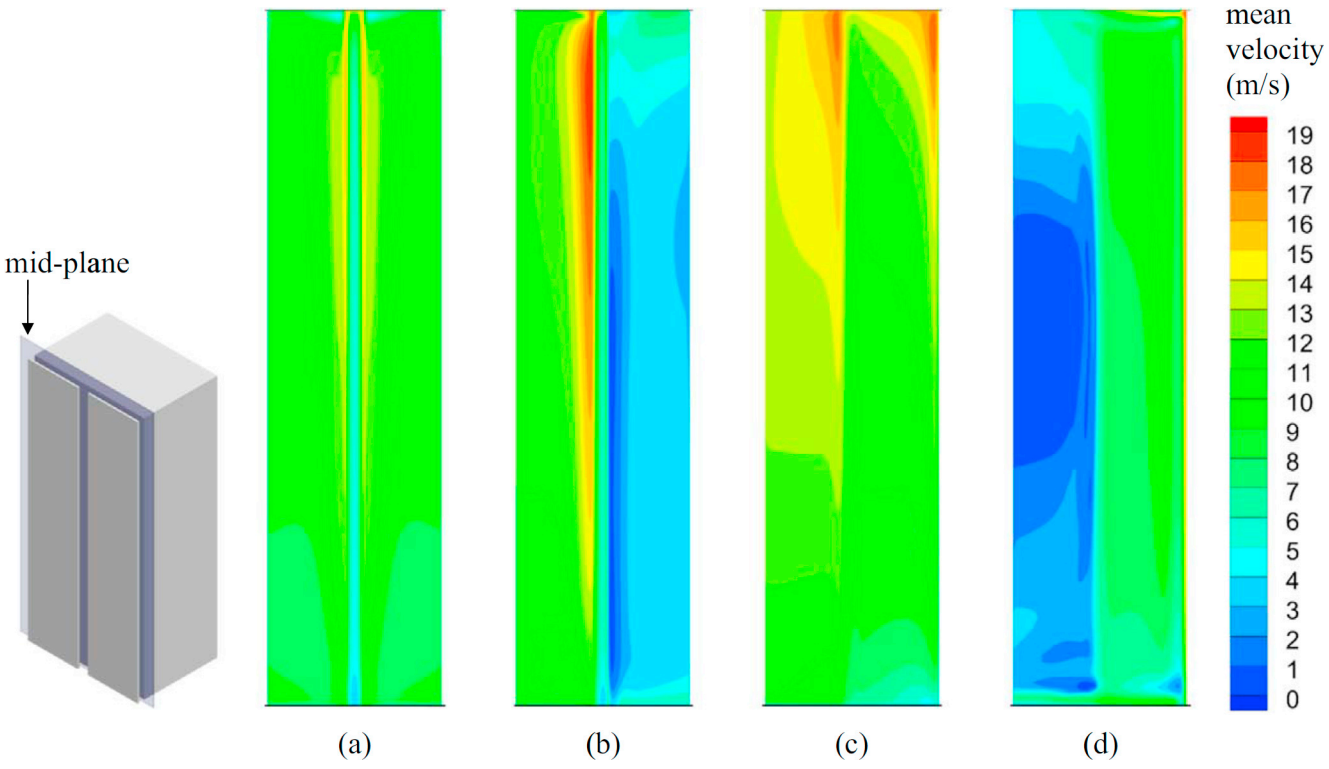

Fig. 11. Mean speed distribution at mid-plane within the cavity for different incident wind directions: (a) 0°, (b) 35°, (c) 65° and (d) 90° (Hassanli et al., 2017).

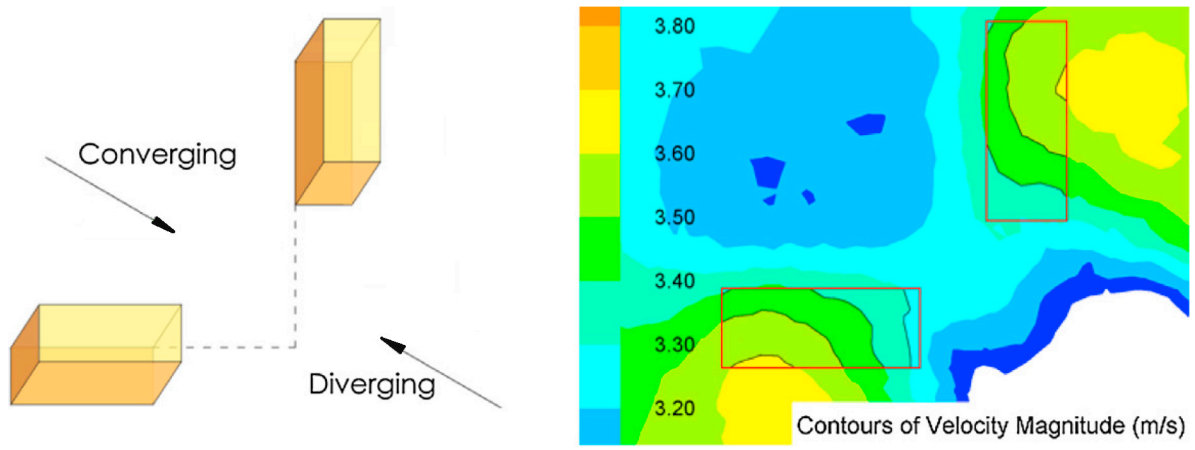

Fig. 12. Converging and diverging distribution of the buildings (left), and example of wind speed distribution above the buildings in converging configuration (right). Adapted from Wang et al. (2015).

They quantify such height as the height which the full swept area of the turbine is separated from the rooftop flow, being at least $z/H = 1.2 - 1.25$. Millward-Hopkins et al. (2012) also quantify the errors inherent in a typical wind resource prediction methodology, which uncertainties accumulated errors can arise up to 30–45% in the final wind speed predictions at potential turbine heights. These errors become even more significant when the cubed relationship of wind power to wind speed is considered. They used LES (standard Smagorinsky model) simulation results produced by Xie et al. (2008) using both ANSYS Fluent and STAR-CD.

Wang et al. (2015) studied the wind accumulation by the Venturi effect in urban environments. They analysed the relationship between wind energy potential and the configuration of two perpendicular buildings by carrying out CFD simulations with different incident wind directions, investigating both converging and diverging positions, as shown in Fig. 12. They considered different building lengths, widths, heights, corner separation distances, incident wind angles and heights for wind harvesting. They validated comparing with a wind tunnel experiment only for wind velocity, using the turbulence models SKE, RNG, realizable $k - \varepsilon$ RANS and the RSM implemented in ANSYS Fluent. According to Wang et al. (2015), the best agreement with the velocity measured in a wind tunnel experiment was found using the SKE model, although such comparison among the models is not shown in their paper, i.e. they only present the results for the SKE. The results for the converging configuration showed that the wind energy potential over the roof increases with larger corner separation, while it decreases for the diverging configuration. For low buildings, the diverging option showed much higher values of wind speed, and small difference between the two configurations was observed for high buildings. A higher energy density is also reported for buildings covering small horizontal surface. According to Wang et al. (2015), most of the converging and diverging cases studied showed a higher wind energy density on the roof, compared with a single isolated building.

Toja-Silva et al. (2016) present an empirical-heuristic optimization of the building-roof shape. They focused in the isolated building shape optimization (commented above), and in the analysis of this building in an urban environment. The effect of the neighboring buildings was investigated considering different heights for the surroundings. A strong influence of the surrounding buildings on the wind flow was observed, and an increase of the TI close to the roof surface is reported. Due to the presence of the surrounding buildings, the TI threshold for HAWT is reached close to the roof surface in all the cases. Therefore, VAWT may be considered close to the roof surface although HAWT can be installed at a higher height ($z/H > 1.05 - 1.15$). Slender shapes were confirmed as the most promising for wind energy exploitation, leading to a higher speed-up and to a lower TI. As shown in Fig. 13 (left), the available wind power is multiplied by 3 due to the optimum building-roof shape compared with the open field, for the isolated building. The available wind power increase show higher values for slender shapes, and it is positive (concentration effect of the wind) for $h/H < 0.8$, where h is the height of the surrounding buildings. It is important to mention that the available wind power is still multiplied by 2 for $h/H = 0.5$ (surrounding buildings half of the target building height). It is also reported that the increase in the inlet velocity has a slightly negative influence. Toja-Silva et al. (2016) also present an example, the instantaneous power generation on the roof for a free-stream velocity (at the building height) of 8.8 m s^{-1}. As shown in Fig. 13 (right), VAWT and HAWT were considered below and above the threshold height, respectively. According to real

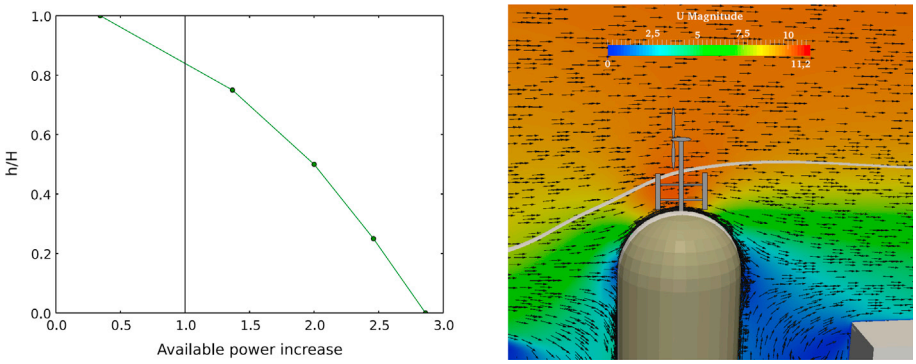

Fig. 13. Available power increase due to the optimum building-roof shape vs. the surrounding builds height (left); and roof-mounted wind turbines superimposed on the velocity field around the building in scale-size agreement (right). Adapted from Toja-Silva et al. (2016).

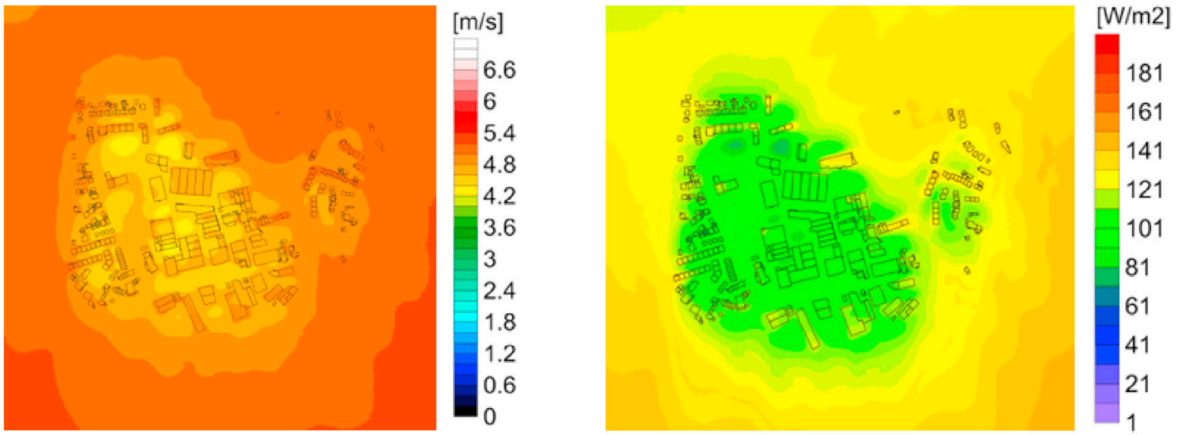

Fig. 14. Spatial distribution of mean wind speed (left) and power density (right) at 10 m above buildings roofs in Cascais, Portugal. Adapted from Simões and Estanqueiro (2016).

measurements on the field carried out by Pagnini et al. (2015) under exactly the same conditions of velocity and TI than those observed at the respective sites on the roof, 8 kW and 9.3 kW of instantaneous power were obtained for the VAWT and HAWT, respectively.

3.3. Real city studies

Tabrizi et al. (2014) carried out CFD simulations of a real industrial area in Port Kennedy (Australia). They used the $k-\omega$ SST RANS turbulence model implemented in ANSYS CFX. They compared the velocity obtained with wind velocity measurements on the site, obtaining a reasonably good agreement. They studied a large-surface low-rise building. The centre of the roof was found to be the best location for a HAWT attending to the horizontality of the wind flow. TKE was not considered in this study.

Simões and Estanqueiro (2016) performed CFD simulations of the wind flow around a real city (Cascais, Portugal) for assessing the urban wind resource. The WindSim software was used, with the SKE RANS turbulence model. As shown in Fig. 14, they computed wind speed and power density on buildings roofs for recommending suitable places for installing wind turbines. The simulation results were compared with measurements on the site, and maximum deviations of the order of 10% and 20% are reported for mean wind speed power density, respectively. Turbulence intensity is not considered in this study.

Yang et al. (2016) conducted CFD simulations and field measurements to evaluate the wind resources available in a real urban area in Taipei (Taiwan). The simulation results were successfully validated for wind speed, direction and turbulence intensity using the realizable $k-\varepsilon$ RANS turbulence model with the software ANSYS Fluent. They found a strong effect of the geometric details of the surrounding buildings on the wind field around the target building, i.e. high-rise buildings in upstream direction tend to block the incoming wind and induce higher turbulence intensity. They recommend installing wind turbines on the windward side of the building, and above the turbulence intensity threshold of 18%. They also analysed different variations of the roofs geometries, in order to improve the wind energy resource. Comparing with simple edge roofs, the curved edge design led to lower turbulence intensity values and higher velocities, yielding a power density increase up to near 90%, as shown in Fig. 15. This conclusion is in agreement with Toja-Silva et al. (2015c).

Liu et al. (2017) carried out CFD simulations of the wind flow in a real urban area, Tianjin city (China). They used the RNG RANS turbulence model implemented in ANSYS. They obtained a reasonably good agreement (around 20% error) between full-scale simulations and rooftop wind velocity measurements on the site. However, as is shown in Fig. 16, for a wind-tunnel reduced-scale model the simulation results overestimate the wind velocity by a factor of two, because the model did not consider the surrounding buildings and, hence, the wind decaying when travelling through the city, even though the exponent on the wind profile was modified for the city terrain. Although they do not focus directly on wind energy, this investigation is of great interest from the urban wind energy point of view because it shows the necessity of either: (a) including upstream buildings (that may affect the wind behaviour in the target area) in CFD simulations of urban environments, or (b) using as reference values wind values taken inside the urban domain instead of free-stream values taken outside of the urban area.

4. CFD simulation of wind turbines on building roofs

4.1. Wake simulation using wind turbine models

Wind turbines models have a great potential for simulating wind turbine wakes on building roofs at a reasonably low computational cost. Therefore, this topic is extensively addressed in the present article.

Several analytical and numerical wind turbine models have been developed since the early days of wind energy, both for single rotors and whole wind farms (in the latter case it is more adequate to refer to them as wind farm parameterizations). An extensive overview of wind turbine models can be found in Vermeer et al. (2003), Sanderse et al. (2011) and Hewitt et al. (2017). Most models have been developed for HAWT. Unless stated otherwise the following explanation applies to HAWT. VAWT will be considered at the end of this section.

In increasing order of complexity, wind turbine models can be roughly divided into analytical, parabolic and numerical (CFD) models. Their range of validity can be expressed as a function of the axial distance from the rotor centre to the area where the wake starts developing. The wake is the area behind a wind turbine where a wind turbine takes momentum from the wind, i.e. the area behind the turbine where the wind speed is reduced. Wakes are typically divided into near and far wakes (Sanderse et al., 2011). The near wake is the region from the rotor plane up to 1D-2D downstream (being D the rotor diameter), where the flow is directly affected by the geometry of the turbine. In the far wake region (>2D downstream the rotor plane) the flow is mainly influenced by the reduced axial velocity and the increased turbulence intensity. Details of the rotor geometry can be ignored in this region. Farther downstream the flow deficit is approximately Gaussian, axisymmetric and self-similar.

Analytical models focus on determining the effects of the wake expansion ignoring the effects of the blades on the flow. They represent the wind deficit behind the turbine using an inverted-hat (Jensen, 1983), cosine (Tian et al., 2015) or Gaussian function (Bastankhah and Porté-Agel, 2014) to describe the wake, providing a simple analytical

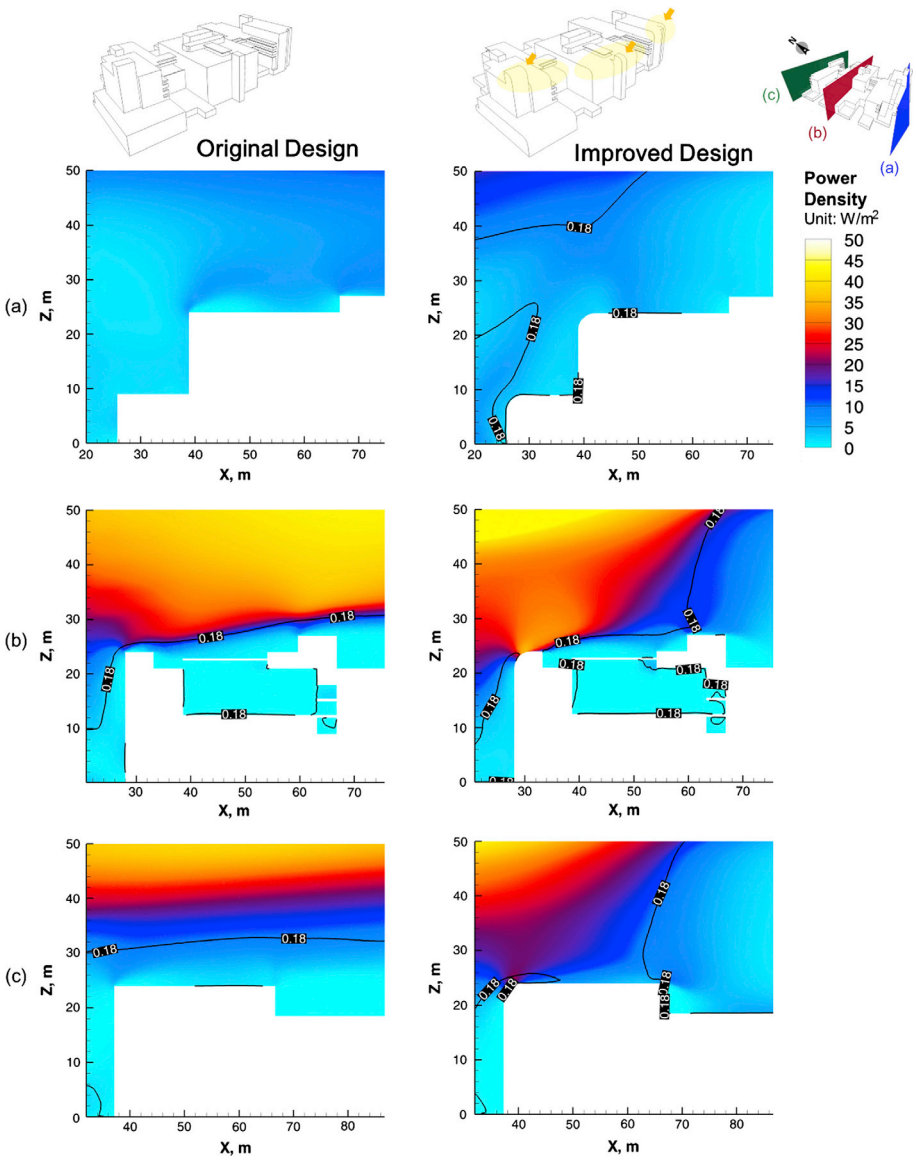

Fig. 15. Power density contours for the original and improved (i.e. curved edged) roof designs of the National Taipei University of Technology at different vertical sections: (a), (b) and (c), respectively. Black line indicates the isoline corresponding to TI = 18%. Adapted from Yang et al. (2016).

expression for the wake deficit which depends on the thrust and rotor diameter of the turbine and an empirical wake expansion coefficient. Analytical models are widely used in commercial software for layout optimization, i.e. WindPro (2017) and Openwind (2017). The approximation on which analytical models are based apply only in the far wake region. For urban wind energy studies, where the number of turbines is usually small and the effects of the buildings strongly influence the wakes of the turbines, a more detailed description of the interaction between the turbine geometry and the incoming flow is usually needed. This restricts the application of analytical models for urban environments.

Parabolic or boundary layer models are based on a parabolization of the Navier-Stokes equations, derived by neglecting the diffusion term and the pressure gradient in the stream-wise direction. A simplified ordinary differential equation can be obtained in this way, which can be solved by space marching algorithms. An example of parabolic model is Ainslie (1988), which solves the parabolized Navier-Stokes equations in polar coordinates with an eddy viscosity model for the turbulence stresses. The UPMWAKE model (Crespo et al., 1994) and WAKEFARM (Schepers, 2003) are extensions of the Ainslie model that do not assume axial symmetry and include corrections for the near wake, respectively. The parabolic approximation is valid in the far wake but, since gradients in the streamwise direction are neglected, parabolic models cannot predict wind speed gradients induced by features of the terrain. This limits their application to moderate or flat terrain topologies. For the remainder of this section we will focus on numerical or CFD models.

The most direct approach (and the most computationally costly) is to include the explicit geometry of the turbine in the computational mesh with a body-fitted grid of the rotor geometry (these works are explained in Section 4.2). As this approach usually requires a large number of cells even for single turbines, simplified versions of the turbine based on momentum theory have been developed. The most commonly used versions are the actuator disc, actuator line and actuator surface models.

The most computationally affordable actuator disc (AD) model is based on one dimensional momentum theory. The motion of the turbine blades is represented as a porous disc that extracts momentum from the incoming flow (Manwell et al., 2009). The force exerted on the flow by the rotating blades is uniformly distributed over the disc and is a function of the thrust coefficient of the wind turbine (C_t). The values of C_t are determined using tabulated values of thrust versus wind speed, which are characteristic of each turbine model. This coefficient is also dependant on

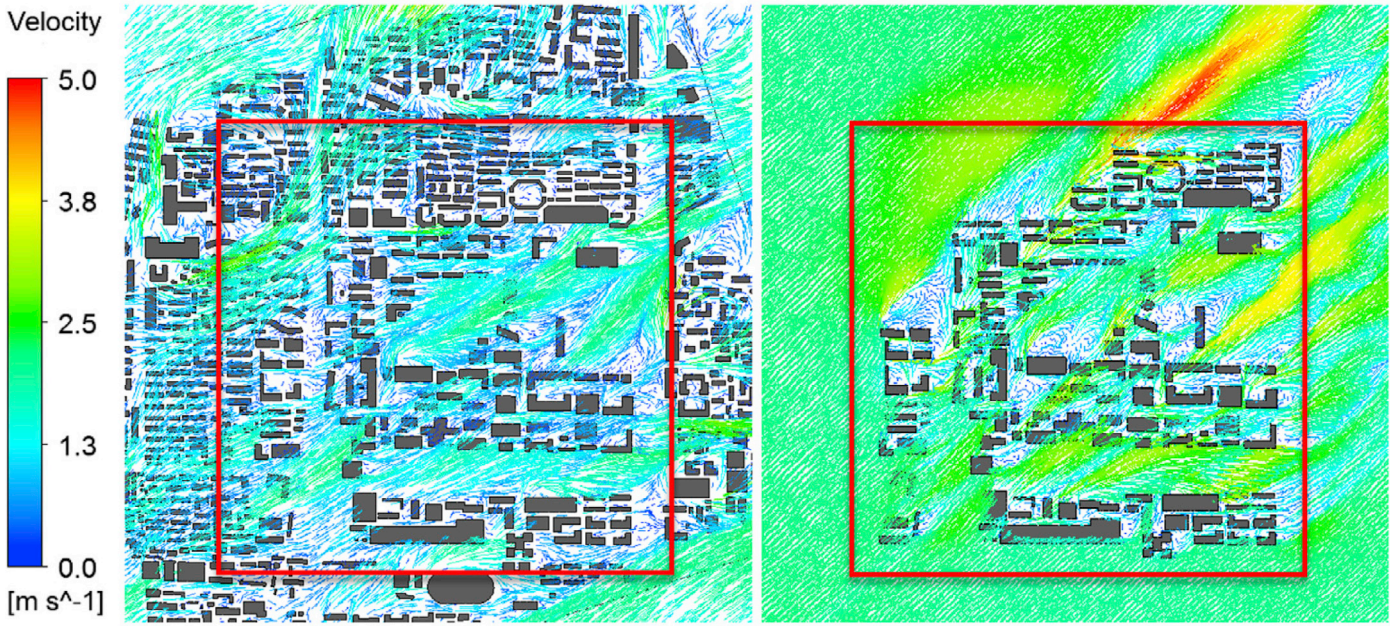

Fig. 16. Differences in the CFD simulation results for a real urban area due to the consideration of the surrounding buildings (Liu et al., 2017): real geometry in Tianjin city, China (left); simplified wind-tunnel scaled geometry that do not consider upstream surrounding buildings (right).

the operating conditions (e.g. air density and turbulence intensity) at which it was measured. The uniformly loaded AD model does not include wake rotation, but reasonable predictions on the far wake region can be obtained with this model.

Originally developed by Sørensen and Shen (1999), the actuator line (AL) model represents the blades as lines. Using blade element momentum (BEM) theory (Manwell et al., 2009), the forces acting on short segments of radial length *dr* are calculated in the axial and tangential directions. The former is just the thrust force (perpendicular to the rotor plane), while the latter is responsible for the torque. Both forces result from a combination of lift and drag forces, which can be determined using tabulated values of lift and drag coefficients, as well as chord length on each radial blade segment represented by the line segments. These values are in a term characteristic of the blade geometry. The forcing term is distributed smoothly over the lines with a Gaussian function around their point of influence in order to avoid singularities and numerical instabilities (Sørensen and Shen, 1999). The AL model offers good predictions in the near wake region, but aerodynamic effects like tip vortices are usually not well predicted. Additionally, the results can be sensitive to the choice of the regularization parameter of the Gaussian smoothing applied on the lines (Herraez et al., 2017).

A simplification of the AL model, which can also be seen as an extension of the AD model, is the AD model with rotation (ADR). As in the AL model, the radial components of the lift and the drag can be computed as a function of the radius, with the forces distributed over annular concentric rings at all radial locations (Ivanell et al., 2008). The main advantage of the ADR model over the AL model is its lower computational cost (Steinfeld et al., 2015). This model suffers from the same deficiencies as its predecessor: tip vortices and other unsteady features of the near wake are not properly captured (Troldborg et al., 2015). However, the ADR model offers a good compromise between accuracy and computational cost, providing reasonable predictions both in the near and far wakes (Steinfeld et al., 2015).

Although the AD and AL models have been widely used in the modelling of wind farms and large wind turbines, there are only a few studies that consider the use of HAWT in the urban environment.

One of the earliest CFD studies on the use of simplified rotor models for urban energy can be found in Mertens et al. (2003). They used the AD theory to model a VAWT (Darrieus) with focus on the wind conditions on the roofs of high-rise buildings and the optimization of the turbine location as function of energy yield. A recent paper by Cooney et al. (2017) simulated the effects of a Vestas V52 wind turbine located near the campus of the Dundalk Institute of Technology in Ireland, but the focus was not in modelling the rotor itself, and rather in characterizing the wind conditions at the site and how this would affect the turbine performance. Micallef et al. (2016) studied the performance of a wind turbine located above a cubic building using the AD model, and found that the strong coupling between the flow around the building and the rotor area can greatly influence the recirculation zone behind the building. This can influence the optimal height at which a turbine should be placed on top of buildings.

Most versions of the simplified models described above consider only horizontal axis wind turbines, but VAWT are very common in urban wind energy. Recently, Bachant et al. (2018) developed an extension of the AL model for VAWT that can be used in both RANS and LES simulations. The model was implemented using the open source code OpenFOAM and validated using two standard reference VAWT. This model was also used by Nuland (2017) to determine the feasibility of using VAWT as a renewable energy source for fish farms. Ferlini et al. (2017) are currently developing a model similar to as Bachant et al. (2018) to study the performance of VAWT in a numerical wind tunnel.

With the increased use of aero generators on the roof of buildings for wind energy exploitation the number of urban wind energy studies that include wind turbine models is likely to grow in the near future, but the only studies found in the literature that simulate a wind turbine on a building roof using a wind turbine model are Mertens at al. (2003) and Micallef et al. (2016), and Nuland (2017) simulated the wind flow around a fish farm barge (see Fig. 17). There is clearly a need of further CFD simulations of urban environments including wind turbine models.

4.2. Real wind turbines on building roofs

Up to date, there are no CFD simulations of conventional HAWT on building roofs. It may be because the economic interest of the application is relatively low when comparing with the very high degree of complexity of the problem and the high computational cost. Therefore, the state-of-the-art shown below refers mainly to non-conventional

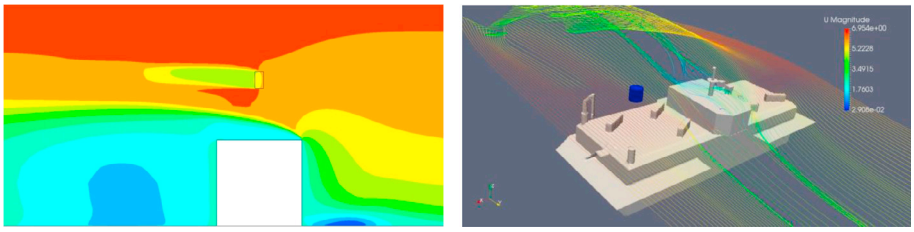

Fig. 17. Left: HAWT model used on a building roof (Micallef et al., 2016). Right: VAWT model (in blue colour) used on a fish farm barge (Nuland, 2017).

and VAWT wind turbines, targeted to the urban wind energy application.

Toja-Silva et al. (2015a) superimposed a ducted wind turbine onto the pressure field obtained from a CFD simulation. As is shown in Fig. 18, since pressure is high (and positive) on the upstream wall and negative on the roof (specially close to the upstream edge), ducted wind turbines are very convenient when having a clear predominant incident wind direction normal to a building wall. Near-normal wind directions are also interesting because conical recirculation vortices may cause a similar pressure distribution around the roof edge.

Zanforlin and Letizia (2015) carried out 2D simulations of a diffuser-augmented Darrieus (VAWT) installed in horizontal position on the top of a pitched roof. They assessed the performance with and without a convergent-divergent diffuser in an open field, and they placed later the turbine on a pitched roof surrounded by a simplified urban area. The simulations were performed using the $k-\omega$ SST URANS turbulence model implemented in ANSYS Fluent. Their results show a significant power increase in skewed winds due to the integration of rooftop and diffuser, and a drastic abatement of torque fluctuations due to the diffuser. Further 3D simulations may be required in order to confirm these results, because it is known that 2D approximation over-predicts the flow yielding incorrect results.

Larin et al. (2016) simulated a Savonius wind turbine installed in horizontal position on the upstream edge of a building, for taking advantage of the wind flow acceleration, as shown in Fig. 19. They show the importance of considering both the building and the wind turbine for a correct power assessment. They carried out a validation using both realizable $k-\varepsilon$ and $k-\omega$ SST URANS turbulence models implemented in ANSYS Fluent. Using the realizable $k-\varepsilon$ model, they obtained more accurate values of the wall friction coefficient, what avoids an over predicted lifting effect on the wind turbine blades. They optimized the Savonius wind turbine for this application by analysing the position, blade number, circumferential length. The optimum geometry, seven bladed turbine with double cut blades, led to a power coefficient of 0.24, about 5–10 times higher than the same turbine placed in open field.

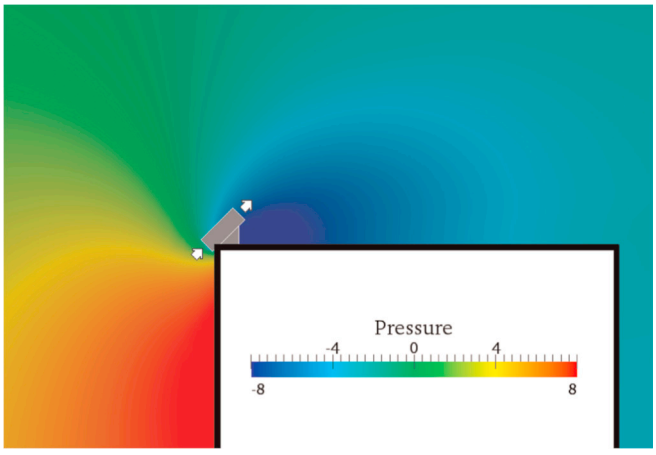

Fig. 18. Ducted wind turbine superimposed onto the pressure field (Toja-Silva et al., 2015a).

Krishnan and Paraschivoiu (2016) continued the work of Larin et al. (2016) by investigating the effect of a diffuser around a Savonius (VAWT) in horizontal position. Such diffuser can be considered inside the same concept proposed by Toja-Silva et al. (2015a) for taking the most of the pressure difference around the upstream edge of the roof, explained above in this Section. The same computational settings as in Larin et al. (2016) were used, i.e. realizable $k-\varepsilon$ RANS model implemented in ANSYS Fluent. They mention that they used a similar mesh density for all the cases (around 6.8 Mcells), but they did not conduct a mesh convergence analysis due to the complexity of the problem. They tested different diffuser shapes (see Fig. 20), yielding a power coefficient improvement from 0.135 to 0.34, what corresponds to a power increase of about 2.5 times with respect to the same Savonius wind turbine in an open field. The authors comment that they are working in a further investigation for the diffuser shape optimization, in order to increase even more the power coefficient. As mentioned in Toja-Silva et al. (2015a) and Larin et al. (2016), this is a very promising application, and Krishnan and Paraschivoiu (2016) suggest a vast scope of future work: e.g. study the effect of change in length of the flange, in length of the turbine roof itself and in the number and shape of the blades, and to investigate the performance and installation strategy under different incident wind directions. Studying this wind turbine on different building-roof shapes should also be added to this list.

Aquino et al. (2017) simulated a pitched-roof building integrated with aero-elastic belts (electromagnetic transduction type). They investigated the effect of different wind conditions (i.e. speed and directions) and aero-elastic belt locations on the device performance. Under the most favorable conditions, the estimated power output generated is 200 mW. The power output is low, but both size and production costs are also low. Therefore, this technology shows an interesting potential for being integrated into the built environment for the small-scale wind energy harvesting. As is shown in Fig. 21, they carried out steady state simulations of the wind belt and the structure on a pitched roof building, and they computed the generated power according to the wind velocity obtained around the aero-elastic belt. They used the SKE RANS turbulence model with ANSYS Fluent.

According to the recent growing literature on the actual behavior of wind turbines in the urban environment (Battisti and Ricci, 2017; Pagnini et al., 2015; Tabrizi et al., 2017; Evans et al., 2017), turbine performance is determined not only by mean wind speed and TKE. At any site, the average wind turbine power output ($\overline{P_w}$) is given by

$$\overline{P_w} = \int_0^\infty P_w(U)p(U)dU\ , \tag{19}$$

where $p(U)$ is the probability density function of the wind speed U, and $P_w(U)$ isthe wind turbine power curve (Manwell et al., 2009). Most determinations of average power assume a Weibull distribution, but it is incorrect in urban settings. Mean wind speed and TKE are taken into account by abovementioned sophisticated RANS modeling. However, there is no literature that exploits the major benefit of LES modeling in terms of its ability to determine the probability density of the wind speed. Therefore, LES has an unexplored great potential for accurate turbine performance evaluation.

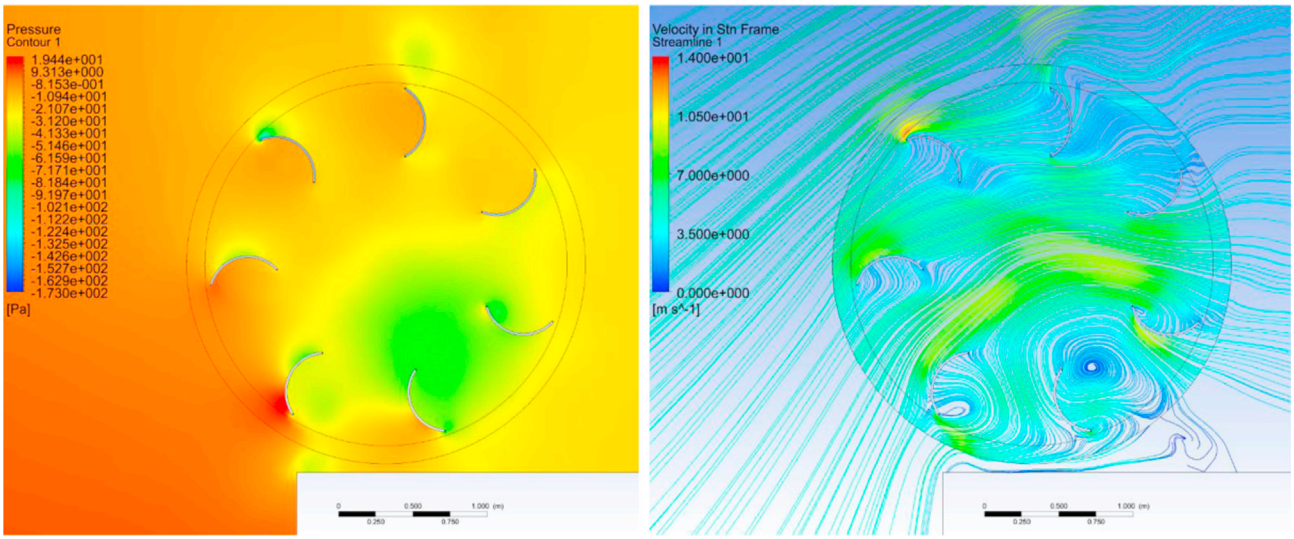

Fig. 19. Pressure contours (left) and streamlines (right) on symmetry plane for seven bladed wind turbine with double cut blades installed on the upstream edge of a building roof (Larin et al., 2016).

5. Summary

This article presents a review about the state-of-the-art of CFD applied to urban wind energy exploitation. The content comprises a technical section that explains CFD aspects relevant for this application, i.e. turbulence modelling, numerical schemes and best practice guidelines. Another core section focuses on the results of building aerodynamics investigations, including the study of the isolated building, simplified urban surroundings and real cities. Finally, the state-of-the-art of the CFD simulation of wind turbines (using both models and real geometries) on building roofs is presented. Table 2 shows a summary of all the investigations related to the state-of-the-art cited in the present review.

Regarding the turbulence models used, the vast majority of investigations were carried out using RANS turbulence models (87% including steady and unsteady simulations). The most used software (i.e. 62% of the total) is the commercial code ANSYS, including Fluent and CFX. Buoyancy is usually not considered in urban wind energy applications, because wind speed is strong enough for being considered as the predominant fluid flow factor. The constant parameters involved in RANS equations have a significant influence on the simulation results in the vicinity of the roof surface. The SKE turbulence model overestimates the TKE in the impinging region of buildings, leading to the underestimation (or complete absence) of the recirculation of the flow on the roof. According to the comparative articles, the RANS turbulence models that better deal with this application are MMK and Durbin. Nonlinear $k-\varepsilon$ models and $k-\omega$ SST produce excessively large recirculation vortexes that extend over the entire roof without attachment. LES models (with inflow turbulence) show better agreement with experiments than RANS models, especially behind the building. However, LES can be successfully validated for TKE focussing only on the roof, in the same way than using RANS. The RSM seems to have good potential for dealing with anisotropic flows, but its accuracy is limited by several closure assumptions needed and, therefore, it is marginally used for this application. Regarding the numerical schemes, is clearly demonstrated that second order accurate schemes (both central differencing and upwind) must be used at least in RANS simulations in order to avoid problems with false diffusion, which may dramatically affect simulation results for TKE. However, for LES, due to physical limitations of the computational meshes, it often needs a blending scheme using a central differencing scheme and small-weighted upwind scheme, i.e. small enough to ensure that the flow field is not overly diffused and at the same time large enough to avoid the occurrence of severe numerical instability. Regarding the best practice guidelines, the reference text is Franke et al. (2007), cited by almost all the researchers in this field.

Regarding the scale of the geometry used for the simulations, the large amount of the cases (70%) were conducted using a full-scale geometry. This is the advantage of CFD simulations in front of experimental measurements. After carrying out an exhaustive validation of the numerical tool by comparing the simulation results with experimental measurements, further simulations (numerical experiments) can be carried out with independency from scaling issues, weather conditions and other physical disturbances.

More than half of the investigations reported (57%) studied isolated buildings. These investigations deal with the wind conditions over roofs with different shapes, its suitability for wind turbines installation and sitting. They search the optimum building-roof shape for the wind energy exploitation attending to both turbulence intensity and the power concentration effect of buildings roofs. Initial works deal with simple roof shapes (i.e. flat, domed, gabled, pyramidal, barrel vaulted and wedged). Further investigations studied additional aspects, like the effect of the roof-edge shape, wall-roof coupling, heuristic variations of the roof shape, building aspect ratio and compatibility between solar and wind energies. The installation of solar panels showed a positive influence on the wind flow (i.e. higher speed and lower TI) for the wind energy exploitation. The influence of the roof edge shape was found to be important, since a similar behavior was observed for both simple edge and cantilever, but advantageous and disadvantageous wind conditions were observed for curved edge and railing, respectively. The area around the upstream edge of flat roofs is identified as the most interesting for the wind energy exploitation due to higher wind power density and lower turbulence intensity. Lower wind velocities are reported for buildings with a higher horizontal surface. Turbulence intensity is identified as the most important factor to decide the most adequate type of wind turbine for a respective location on the roof. Values of TI between 0.15 and 0.25 are mentioned as the threshold for installing a conventional HAWT in order to prevent damages, depending on either European Wind Turbine Standards II or International Electrotechnical Commission Standard 61400-2 (less restrictive) is considered. According to the literature cited, the threshold height for a HAWT over a flat roof is around 30% of the building height, and VAWT is more adequate for being installed below this threshold height. Such threshold height may vary depending on the surrounding buildings. Flat roof showed more advantageous conditions than sharp roofs (i.e. pitched and shed), but curved shapes (e.g. vaulted and spherical) showed the best conditions with a big difference. An exactly spherical roof coupled with a cylindrical wall was identified as the optimum for the wind energy exploitation, attending to both speed-

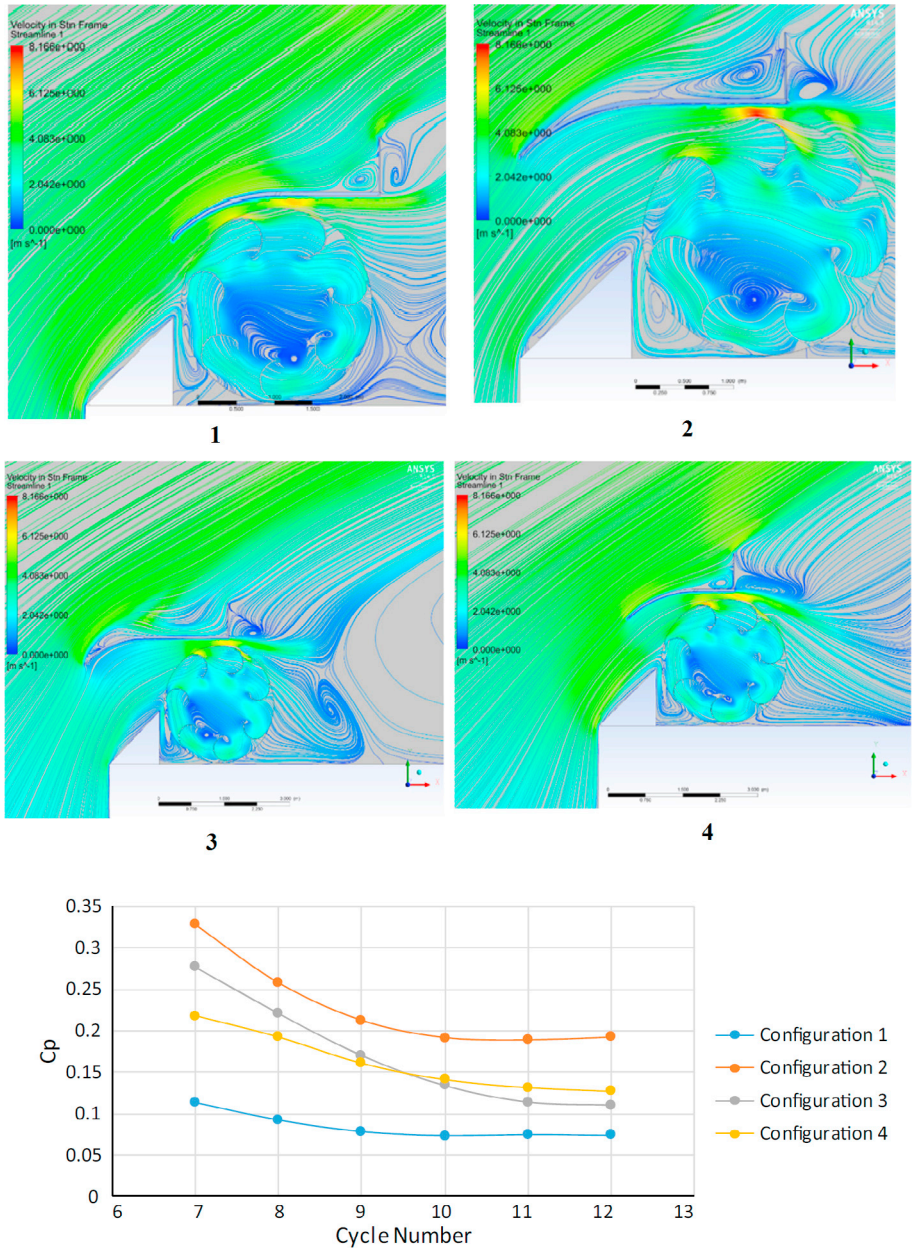

Fig. 20. Streamlines around the wind turbine (top) and power coefficient (Cp) per cycle (bottom) for different configurations of the diffusor. Adapted from Krishnan and Paraschivoiu (2016).

up and TI. As a new application, it is proposed a double-skin façade system with strategic openings, which can lead to high-speed values and low TI (even lower than free-stream).

Analyses of simplified urban patterns and studies of a target building with simplified surrounding were conducted in 29% of the cases reported, respectively. There is a consensus regarding the very significant effect of the surrounding buildings on the wind flow around the target building. Such effect can be negative but also positive. The uncertainties accumulated errors in wind resource prediction due to not considering adequately the urban environment can arise up to 45%, and they can become even more significant when the cubed relationship of wind power to wind speed is considered. Using a semi-log wind profile is an alternative for isolated buildings in order to improve the canopy velocity prediction, reducing the error mentioned above. The available wind power on the optimum building-roof shape (i.e. spherical roof with a cylindrical wall) can be multiplied by 3 (comparing with open field) for the isolated building, and by 2 when the surrounding buildings have half of the target building height.

The studies that deal with a real urban area only represent the 14% of the total reported in this review, because their conclusions are only applicable (normally) to the particular case studied. These investigations present numerical simulations of a part of a real city, and compare velocity values with experimental measurements on the site. Wind turbines positioning on real building roofs is also discussed. In a comparison between the simulation results for an urban region and for a small area inside such region, was observed that the simulation results for the small area overestimated the wind velocity by a factor of two, because the model did not consider the surrounding buildings. Therefore, these CFD simulations must include surrounding buildings or use wind reference values taken inside the urban domain instead of free-stream values.

Wind turbines models have a great potential for simulating wind turbine wakes on building roofs at a reasonably low computational cost. Several analytical and numerical wind turbine models have been developed for HAWT, but VAWT are more interesting for urban wind energy

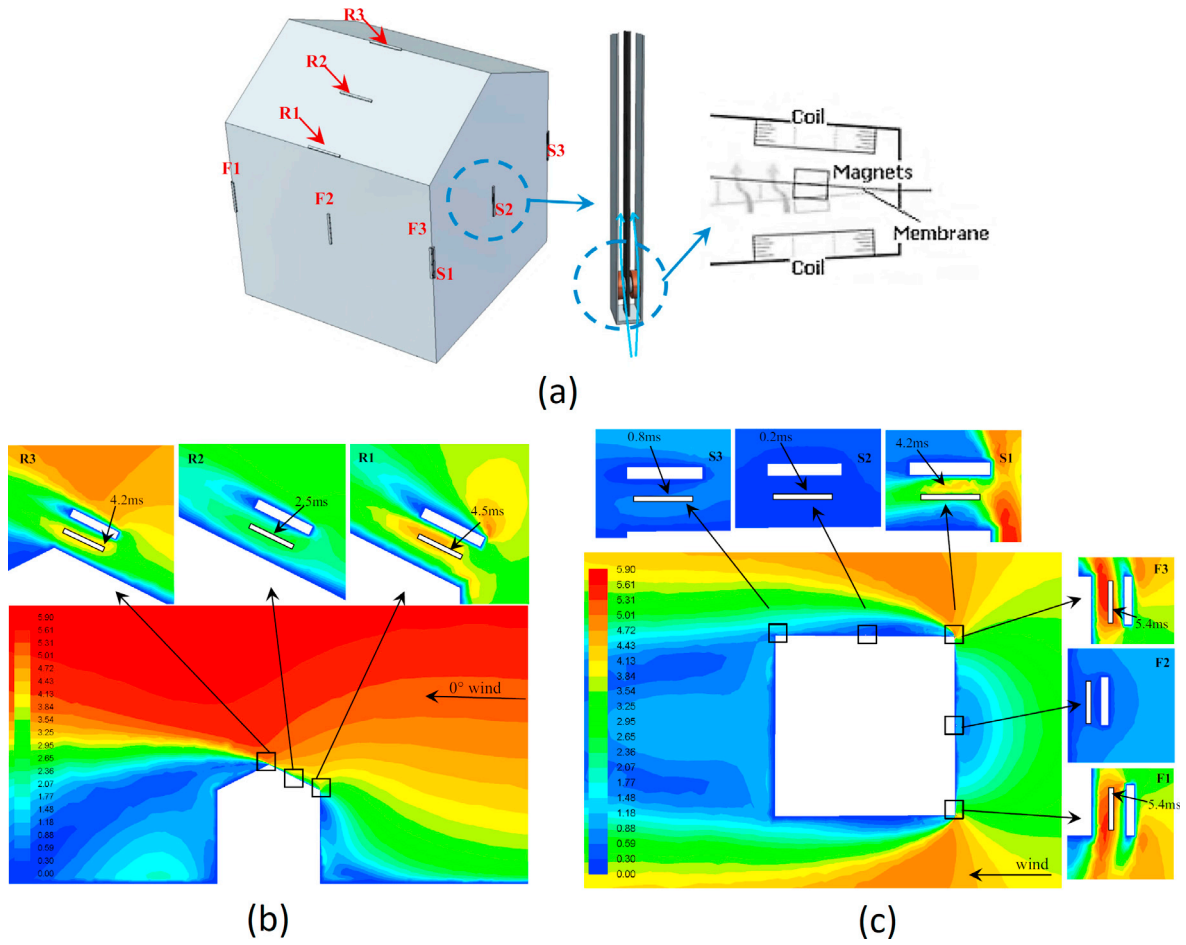

Fig. 21. CFD simulation of aero-elastic belts on a building (Aquino et al., 2017): geometry of the building with the aero-elastic belts (a); contours of wind speed around the aero-elastic belts on the roof (b) and on the building walls (c).

applications. Such models consist in simplified versions of the turbine based on momentum theory. The most commonly used versions are the actuator disc, actuator line and actuator surface models. Although these models have been widely used in the modelling of wind farms and large wind turbines, there are only a few studies that consider the use of wind turbines in the urban environment. With the increased use of aero generators on the roof of buildings for wind energy exploitation the number of urban wind energy studies that include wind turbine models is likely to grow in the near future but, as stated above, only 3 studies were found in the literature that conducted CFD simulations using wind turbines models in the built environment.

CFD simulations of real wind turbines on buildings roofs were only carried out for non-conventional HAWT and VAWT. The most relevant concepts deal with taking the most of the pressure difference around the upstream edge of the building roof (i.e. ducted wind turbine and diffuser), and of the recirculation of the flow on the roof (i.e. Savonius VAWT in horizontal position). The power coefficient of such wind turbine can be 10 times higher than in open field conditions. Another interesting application presented is the use of aero-elastic belts for small-scale power generation.

Some recommendations for further investigations arise from this literature review:

- The study of the threshold height for conventional buildings (e.g. flat roof) was not carried out considering the effect of the surrounding buildings. A good practice guideline for wind turbine installation may be useful, including a table for different general cases. Such guideline can be developed using CFD simulations.
- The study of the wind energy exploitation through passages inside buildings has a great interest due to the pressure difference. In the same way than the double-skin façade, additional innovative configurations and systems can be further studied and optimized.
- There are very few studies in the literature including wind turbine models in urban environments. More studies are definitively required.
- CFD simulations of conventional HAWT installed on building roofs, using real geometry. To the authors' knowledge, no such studies are yet available in the literature.
- LES has an unexplored great potential for accurate turbine performance evaluation, due to its ability to determine the probability density of the wind speed.
- Further development and optimization of VAWT in horizontal position, as this application shows a great potential for the urban environment.

References

Abohela, I., 2012. Effect of Roof Shape, Wind Direction, Building Height and Urban Configuration on the Energy Yield and Positioning of Roof Mounted Wind Turbines. Ph.D. Thesis (School of Architecture, Planning and Landscape, Newcastle University, United Kingdom).

Abohela, I., Hamza, N., Dudek, S., 2013. Effect of roof shape, wind direction, building height and urban configuration on the energy yield and positioning of roof mounted wind turbines. Renew. Energy 50, 1106–1118.

Ainslie, J., 1988. Calculating the flow field in the wake of wind turbines. J. Wind Eng. Ind. Aerod. 27, 213–224.

ANSYS, 2017a. Reynolds stress model (RSM) theory. https://www.sharcnet.ca/Software/Fluent6/html/ug/node490.htm (accessed on 12/30/2017).

ANSYS, 2017b. Computational fluid dynamics (CFD) software. http://www.ansys.com/products/fluids (accessed on 12/30/2017).
Aquino, A.I., Calautit, J.K., Hughes, B.R., 2017. Integration of aero-elastic belt into the built environment for low-energy wind harnessing: current status and a case study. Energy Convers. Manag. 149, 830–850.
Architectural Institute of Japan, 2017. Guidebook for Practical Applications of CFD to Pedestrian Wind Environment Around Buildings. http://www.aij.or.jp/jpn/publish/cfdguide/index_e.htm (accessed on 12/30/2017).
Bachant, P., Goude, A., Wosnik, M., 2018. Actuator line modeling of vertical-axis turbines. Energies, under review. Available online: https://www.researchgate.net/publication/301896257_Actuator_line_modeling_of_vertical-axis_turbines (accessed on 06/27/2018).
Bakker, A., 2016. Applied computational fluid dynamics. http://www.bakker.org/dartmouth06/engs150/05-solv.pdf (accessed on 06/27/2018).
Balogh, M., Parente, A., Benocci, C., 2012. RANS simulation of ABL flow over complex terrains applying an Enhanced k-ε model and wall function formulation: implementation and comparison for Fluent and OpenFOAM. J. Wind Eng. Ind. Aerod. 106, 360–368.
Bastankhah, M., Porté-Agel, F., 2014. A new analytical model for wind-turbine wakes. Renew. Energy 70, 116–123.
Batchelor, G.K., 1988. An Introduction to Fluid Dynamics. Cambridge University Press, Cambridge.
Battisti, L., Ricci, M., 2017. Wind Energy Exploitation in Urban Environment. TUrbWind 2017 Colloquium. Springer International Publishing.
Bechmann, A., Sørensen, N.N., 2010. Hybrid RANS/LES method for wind flow over complex terrain. Wind Energy 13, 36–50.
Beller, C., 2011. Urban Wind Energy. Ph.D. Thesis. Risø Nationallaboratoriet for Bæredygtig Energi, Danmarks Tekniske Universitet (DTU), Denmark.
Blocken, B., 2014. 50 years of Computational Wind Engineering: past, present and future. J. Wind Eng. Ind. Aerod. 129, 69–102.
Blocken, B., Carmeliet, J., 2008. Pedestrian wind conditions at outdoor platforms in a high-rise apartment building: generic sub-configuration validation, wind comfort assessment and uncertainty issues. Wind Struct. 11, 51–70.
Blocken, B., Janssen, W.D., van Hooff, T., 2012. CFD simulation for pedestrian wind comfort and wind safety in urban areas: general decision framework and case study for the Eindhoven University campus. Environ. Model. Software 30, 15–34.
Blocken, B., Stathopoulos, T., van Beeck, J.P.A.J., 2016. Pedestrian-level wind conditions around buildings: review of wind-tunnel and CFD techniques and their accuracy for wind comfort assessment. Build. Environ. 100, 50–81.
Center for Research on Innovative Simulation Software, 2017. FrontFlow/red. http://www.ciss.iis.u-tokyo.ac.jp/english/dl/index.php (accessed on 12/30/2017).
Chen, J., Viatte, C., Hedelius, J.K., Jones, T., Franklin, J.E., Parker, H., Gottlieb, E.W., Wennberg, P.O., Dubey, M.K., Wofsy, S.C., 2016. Differential column measurements using compact solar-tracking spectrometers. Atmos. Chem. Phys. 16, 8479–8498.
Cheng, H., Castro, I.P., 2002. Near wall flow over urban-like roughness. Boundary-Layer Meteorol. 104, 229–259.
Cheng, Y., Lien, F.S., Yee, E., Sinclair, R., 2003. A comparison of large eddy simulations with a standard k-ε Reynolds-averaged Navier-Stokes model for the prediction of a fully developed turbulent flow over a matrix of cubes. J. Wind Eng. Ind. Aerod. 91, 1301–1328.
Chicco, G., Mancarella, P., 2009. Distributed multi-generation: a comprehensive view. Renew. Sustain. Energy Rev. 13, 535–551.
Cooney, C., Byrne, R., Lyons, W., O'Rourke, F., 2017. Performance characterisation of a commercial-scale wind turbine operating in an urban environment, using real data. Energy for Sustainable Development 36, 44–54.
Craft, T.J., Launder, B.E., Suga, K., 1996. Development and application of a cubic eddy-viscosity model of turbulence. Int. J. Heat Fluid Flow 17, 108–115.
Crespo, A., Manuel, F., Moreno, D., Fraga, E., Hernández, J., 1985. Numerical analysis of wind turbine wakes. In: Proceedings of Delphi Workshop on Wind Energy Applications, Delphi (Greece), pp. 15–25.
Crespo, A., Chacón, L., Hernández, J., Manuel, F., Grau, J.C., 1994. UPMPARK: a parabolic 3D code to model wind farms. In: Proceedings of EWEC'94, Thessaloniki (Greece), pp. 454–459.
Du, Y., Mak, C.M., Liu, J., Xia, Q., Niu, J., Kwok, K.C.S., 2017. Effects of lift-up design on pedestrian level wind comfort in different building configurations under three wind directions. Build. Environ. 117, 84–99.
Durbin, P.A., 1996. On the k-ε stagnation point anomaly. Int. J. Heat Fluid Flow 17, 89–90.
Ehrhard, J., Moussiopoulos, N., 2000. On a new nonlinear turbulence model for simulating flows around building shaped structures. J. Wind Eng. Ind. Aerod. 88, 91–99.
Encraft, 2009. Warwick wind trials project. Final report. Available online: http://www.microwindturbine.be/Rapportering_files/Warwick+Wind+Trials+Final+Report+%281%29.pdf (accessed on 06/20/2018).
Eriksson, S., Bernhoff, H., Leijon, M., 2008. Evaluation of different turbine concepts for wind power. Renew. Sustain. Energy Rev. 12, 1419–1434.
Evans, S.P., Anup, K.C., Bradney, D.R., Urmee, T.P., Whale, J., Clausen, P.D., 2017. The suitability of the IEC 61400-2 wind model for small wind turbines operating in the built environment. Renewable Energy and Environmental Sustainability 2, 31.
Ferlini, M., Bernini, L., Schito, P., Zasso, A., 2017. CFD model of a vertical-axis wind turbine in open-jet wind-tunnel. In: Fifth Symposium on OpenFOAM in Wind Energy, Pamplona.
Ferziger, J.H., Peric, M., 2002. Computational Methods for Fluid Dynamics, third ed. Springer.
Franke, J., Hellsten, A., Schlünzen, H., Carissimo, B., 2007. Best Practice Guideline for the CFD Simulation of Flows in the Urban Environment. COST Action 732, Quality Assurance and Improvement of Microscale Meteorological Models. COST Office, Brussels.
Germano, M., Piomelli, U., Moin, P., Cabot, W.H., 1991. A dynamic subgrid-scale eddy viscosity model. Phys. Fluid. Fluid Dynam. 3, 1760–1765.
Gousseau, P., Blocken, B., van Heijst, G.J.F., 2013. Quality assessment of large-eddy simulation of wind flow around a high-rise building: validation and solution verification. Comput. Fluids 79, 120–133.
Hassanli, S., Hu, G., Kwok, K.C.S., Fletcher, D.F., 2017. Utilizing cavity flow within double skin façade for wind energy harvesting in buildings. J. Wind Eng. Ind. Aerod. 167, 114–127.
Heath, M.A., Walshe, J.D., Watson, S.J., 2007. Estimating the potential yield of small building-mounted wind turbines. Wind Energy 10, 271–287.
Herraez, I., Micallef, D., van Kuik, G.A.M., 2017. Influence of the conservative rotor loads on the near wake of a wind turbine. J. Phys. Conf. 854. Wake Conference 2017.
Hewitt, S., Margetts, L., Revell, A., 2017. Building a digital wind farm. Arch. Comput. Meth. Eng. 24, 1–21.
Hirsch, C., 2007. Numerical Computation of Internal & External Flows. The Fundamentals of Computational Fluid Dynamics, second ed. Elsevier.
International Electrotechnical Commission, IEC, 2006. International standards IEC 61400-2. Wind turbines - part 2: design requirements for small wind turbines.
Ishugah, T.F., Li, Y., Wang, R.Z., Kiplagat, J.K., 2014. Advances in wind energy resource exploitation in urban environment: a review. Renew. Sustain. Energy Rev. 37, 613–626.
Ivanell, S., Mikkelsen, R., Sørensen, J.N., Henningson, D., 2008. Validation of Methods Using EllipSys3D. Technical Report. KTH Mechanics, Stockholm.
Jensen, N.O., 1983. A Note on Wind Generator Interaction. Risø Report M-2411. Risø National Laboratory, Roskilde.
Khare, V., Nema, S., Baredar, P., 2016. Solar-wind hybrid renewable energy system: a review. Renew. Sustain. Energy Rev. 58, 23–33.
Kono, T., Kogaki, T., 2012. Numerical investigation of wind conditions over a rectangular prism-shaped building for mounting small wind turbines. Wind Eng. 36, 111–122.
Kono, T., Kogaki, T., Kiwata, T., 2016. Numerical investigation of wind conditions for roof-mounted wind turbines: effects of wind direction and horizontal aspect ratio of a high-rise cuboid building. Energies 9, 907.
Krishnan, A., Paraschivoiu, M., 2016. 3D analysis of building mounted VAWT with diffuser shaped shroud. Sustainable Cities and Society 27, 160–166.
Larin, P., Paraschivoiu, M., Aygun, C., 2016. CFD based synergistic analysis of wind turbines for roof mounted integration. J. Wind Eng. Ind. Aerod. 156, 1–13.
Launder, B.E., Kato, M., 1993. Modeling flow-induced oscillations in turbulent flow around a square cylinder. In: ASME Fluid Engineering Conference.
Launder, B.E., Reece, G.J., Rodi, W., 1975. Progress in the development of a Reynolds-stress turbulence closure. J. Fluid Mech. 68, 537–566.
Ledo, L., Kosasih, P.B., Cooper, P., 2011. Roof mounting site analysis for micro-wind turbines. Renew. Energy 36, 1379–1391.
Lilly, D.K., 1992. A proposed modification of the Germano subgrid-scale model. Phys. Fluid. Fluid Dynam. 4, 633–635.
Liu, S., Pan, W., Zhang, H., Cheng, X., Long, Z., Chen, Q., 2017. CFD simulations of wind distribution in an urban community with a full-scale geometrical model. Build. Environ. 117, 11–23.
Lu, L., Ip, K.Y., 2009. Investigation on the feasibility and enhancement methods of wind power utilization in high-rise buildings of Hong Kong. Renew. Sustain. Energy Rev. 13, 450–461.
Manwell, J.F., McGowan, J.G., Rogers, A.L., 2009. Wind Energy Explained: Theory, Design and Application, second ed. John Wiley & Sons, Chichester.
Meng, T., Hibi, K., 1998. Turbulent measurements of the flow field around a high-rise building. J. Wind Eng. 76, 55–64.
Menter, F.R., 1994. Two-equation eddy-viscosity turbulence models for engineering applications. AIAA J. 32, 1598–1605.
Mertens, S., 2006. Wind Energy in the Built Environment, Concentrator Effects of Buildings. Ph.D. Thesis. Technische Universiteit Delft (TU Delft), Netherlands.
Mertens, S., van Kuik, G., van Bussel, G., 2003. Performance of an H-Darrieus in the skewed flow on a roof. J. Sol. Energy Eng. 125, 433–440.
Micallef, D., Sant, T., Ferreira, C., 2016. The influence of a cubic building on a roof mounted wind turbine. J. Phys. Conference Series, 753, The Science of Making Torque from Wind (TORQUE 2016).
Millward-Hopkins, J.T., Tomlin, A.S., Ma, L., Ingham, D., Pourkashanian, M., 2012. The predictability of absove roof wind resource in the urban roughness sublayer. Wind Energy 15, 225–243.
Millward-Hopkins, J.T., Tomlin, A.S., Ma, L., Ingham, D.B., Pourkashanian, M., 2013. Mapping the wind resource over UK cities. Renew. Energy 55, 202–211.
Mohamed, M.A., Sherry, M., P. du Plessix, Wood, D.H., Martinuzzi, R.J., 2018. Measurements to assess simple RANS model behaviour in stagnating flow. Int. J. Heat Fluid Flow 70, 226–236.
Murakami, S., Iizuka, S., Ooka, R., 1999. CFD analysis of turbulent flow past square cylinder using dynamic LES. J. Fluid Struct. 13, 1097–1112.
Murthy, K.S.R., Rahi, O.P., 2017. A comprehensive review of wind resource assessment. Renew. Sustain. Energy Rev. 72, 1320–1342.
Nozu, T., Tamura, T., 2012. LES of turbulent wind and gas dispersion in a city. J. Wind Eng. Ind. Aerod. 104–106, 492–499.
Nuland, S.E., 2017. Wind turbine installation on offshore fish farm feed barge. In: Fifth Symposium on OpenFOAM in Wind Energy, Pamplona.
Ono, Y., Tamura, T., 2002. Large eddy simulation using a curvilinear coordinate system for the flow around a square cylinder. Wind Struct. 5, 369–378.
OpenFOAM, 2017. The Open Source CFD Toolbox. http://www.openfoam.com/. (Accessed 30 December 2017).

Openwind (2017). http://software.awstruepower.com/openwind/(accessed on 12/30/2017).
Pagnini, L.C., Burlando, M., Repetto, M.P., 2015. Experimental power curve of small-size wind turbines in turbulent urban environment. Appl. Energy 154, 112–121.
Panofsky, H., Dutton, J., 1984. Atmospheric Turbulence. Wiley, New York.
Pierik, J.T.G., Dekker, J.W.M., Braam, H., Bulder, B.H., Winkelaar, D., Larsen, G.C., Morfiadakis, E., Chaviaropoulos, P., Derrick, A., Molly, J.P., 1999. Wind energy for the next millennium. In: Proceedings of the European Wind Turbine Standards II (EWTS-II). James and James Science Publishers, London.
Rákai, A., Kristóf, G., Franke, J., 2014. Sensitivity analysis of micro scale obstacle resolving models for an idealized Central European city center, Michel-Stadt. Quarterly Journal of the Hungarian Meteorological Service 118, 53–77.
Richardson, L.F., 1911. The approximate arithmetical solution by finite differences of physical problems involving differential equations with an application to the stresses in a masonry dam. Philosophical Transactions of the Royal Society A 210, 459–470.
Roache, P.J., 1998. Verification of codes and calculations. AIAA J. 36, 696–702.
Rodi, W., 1997. Comparison of LES and RANS calculations of the flow around bluff bodies. J. Wind Eng. Ind. Aerod. 69–71, 55–75.
Sanderse, B., van der Pijl, S.P., Koren, B., 2011. Review of the computational fluid dynamics for wind turbine aerodynamics. Wind Energy 14, 799–819.
Santiago, J.L., Martilli, A., Martín, F., 2007. CFD simulation of air flow over a regular array of cubes. Part I: three-dimensional simulation of the flow and validation with wind-tunnel measurements. Boundary-Layer Meteorol. 122, 609–634.
Schepers, J.G., 2003. ENDOW: validation and improvement of ECN's wake model. Technical report ECN-C&ndash 03–034.
Shao, J., Liu, J., Zhao, J., 2012. Evaluation of various non-linear k-ε models for predicting wind flow around an isolated high-rise building within the surface boundary layer. Build. Environ. 57, 145–155.
Shih, T.H., Zhu, J., Lumley, J.L., 1993. A realizable Reynolds Stress Algebraic Equation Model. NASA Tech Memo 105993.
Siemens, 2017. STAR-CD. http://mdx.plm.automation.siemens.com/star-cd (accessed on 12/30/2017).
Simões, T., Estanqueiro, A., 2016. A new methodology for urban wind resource assessment. Renew. Energy 89, 598–605.
Smagorinsky, J., 1991. General circulation experiments with the primitive equations. Mon. Weather Rev. 91, 99–164.
Sohankar, A., Davidson, L., Norberg, C., 1999. Large eddy simulation of flow past a square cylinder: comparison of different subgrid scale models. J. Fluid Eng. 122, 39–47.
Sørensen, N.N., 1995. General Purpose Flow Solver Applied to Flow over Hills. Risø-r-827-(EN). Risø National Laboratory, Roskilde, Denmark.
Sørensen, J.N., Shen, W.Z., 1999. Computation of wind turbine wakes using combined Navier-Stokes/actuator-line methodology. In: 1999 European Wind Energy Conference and Exhibition, Stockholm.
Steinfeld, G., Witha, B., Dörenkämper, M., Gryschka, M., 2015. High-resolution large-eddy simulations for the analysis of flow conditions in offshore wind farms. Promet-Meteorologische Fortbildung 39, 163–180.
Tabrizi, A.B., Whale, J., Lyons, T., Urmee, T., 2014. Performance and safety of rooftop wind turbines: use of CFD to gain insight into inflow conditions. Renew. Energy 67, 242–251.
Tabrizi, A.B., Whale, J., Lyons, T., Urmee, T., Peinke, J., 2017. Modelling the structural loading of a small wind turbine at a highly turbulent site via modifications to the Kaimal turbulence spectra. Renew. Energy 105, 288–300.
Tian, L., Zhu, W., Shen, W., Zhao, N., Shen, Z., 2015. Development and validation of a new two-dimensional wake model for wind turbines. J. Wind Eng. Ind. Aerod. 137, 90–99.
Toja Silva, F., 2015. Urban Wind Energy: Empirical Optimization of High-rise Building Roof Shape for the Wind Energy Exploitation. Ph.D. Thesis. Escuela Técnica Superior de Ingenieros Aeronáuticos, Universidad Politécnica de Madrid (UPM), Spain. http://oa.upm.es/38529/.
Toja-Silva, F., Colmenar-Santos, A., Castro-Gil, M., 2013. Urban wind energy exploitation systems: behavior under multidirectional flow conditions - opportunities and challenges. Renew. Sustain. Energy Rev. 24, 364–378.
Toja-Silva, F., Peralta, C., Lopez-Garcia, O., Navarro, J., Cruz, I., 2015a. Roof region dependent wind potential assessment with different RANS turbulence models. J. Wind Eng. Ind. Aerod. 142, 258–271.
Toja-Silva, F., Peralta, C., Lopez-Garcia, O., Navarro, J., Cruz, I., 2015b. Effect of roof-mounted solar panels on the wind energy exploitation on high-rise buildings. J. Wind Eng. Ind. Aerod. 145, 123–138.
Toja-Silva, F., Peralta, C., Lopez-Garcia, O., Navarro, J., Cruz, I., 2015c. On roof geometry for urban wind energy exploitation in high-rise buildings. Computation 3, 299–325.
Toja-Silva, F., Peralta, C., Lopez-Garcia, O., Navarro, J., Cruz, I., 2016. An empirical-heuristic optimization of the building-roof geometry for urban wind energy exploitation on high-rise buildings. Appl. Energy 164, 769–794.
Toja-Silva, F., Chen, J., Hachinger, S., Hase, F., 2017. CFD simulation of CO_2 dispersion from urban thermal power plant: analysis of turbulent Schmidt number and comparison with Gaussian plume model and measurements. J. Wind Eng. Ind. Aerod. 169, 177–193.
Toja-Silva, F., Pregel-Hoderlein, C., Chen, J., 2018. On the urban geometry generalization for CFD simulation of gas dispersion from chimneys: comparison with Gaussian plume model. J. Wind Eng. Ind. Aerod. 177, 1–18.
Tominaga, Y., Stathopoulos, T., 2013. CFD simulation of near-field pollutant dispersion in the urban environment: a review of current modeling techniques. Atmos. Environ. 79, 716–730.
Tominaga, Y., Mochida, A., Murakami, S., Sawaki, S., 2008a. Comparison of various revised k-ε models and LES applied to flow around a high-rise building model with 1: 1:2 shape placed within the surface boundary layer. J. Wind Eng. Ind. Aerod. 96, 389–411.
Tominaga, Y., Mochida, A., Yoshie, R., Kataoka, H., Nozu, T., Yoshikawa, M., Shirasawa, T., 2008b. AIJ guidelines for practical applications of CFD to pedestrian wind environment around buildings. J. Wind Eng. Ind. Aerod. 96, 1749–1761.
Troldborg, N., Zahle, F., Réthoré, P.-E., Sørensen, N.N., 2015. Comparison of wind turbine wake properties in non-sheared inflow predicted by different computational fluid dynamics rotor models. Wind Energy 18, 1239–1250.
Tsuchiya, M., Murakami, S., Mochida, A., Kondo, K., Ishida, Y., 1997. Development of a new k-ε model for flow and pressure fields around bluff body. J. Wind Eng. Ind. Aerod. 67–68, 169–182.
van Hooff, T., Blocken, B., 2010. Coupled urban wind flow and indoor natural ventilation modelling on a high-resolution grid: a case study for the Amsterdam ArenA stadium. Environ. Model. Software 25, 51–65.
Van-Driest, E.R., 1956. On turbulent flow near a wall. J. Aeronaut. Sci. 23, 1007–1011.
Vermeer, L.J., Sørensen, N.O., Crespo, A., 2003. Wind turbine wake aerodynamics. Prog. Aero. Sci. 39, 467–510.
Walker, S.L., 2011. Building mounted wind turbines and their suitability for the urban scale - a review of methods of estimating urban wind resource. Energy Build. 43, 1852–1862.
Wang, B., Cot, L.D., Adolphe, L., Geoffroy, S., Morchain, J., 2015. Estimation of wind energy over roof of two perpendicular buildings. Energy Build. 88, 57–67.
Wang, Q., Wang, J., Hou, Y., Yuan, R., Luo, K., Fan, J., 2018. Micrositing of roof mounting wind turbine in urban environment: CFD simulations and lidar measurements. Renew. Energy 115, 1118–1133.
WindPRO, 2017. Remote sensing data and other data for download in WindPRO. http://www.emd.dk/files/windpro/WindPRO_OnlineData.pdf (accessed on 12/30/2017).
WindSim, 2017. Products. https://www.windsim.com/products.aspx (accessed on 12/30/2017).
Xie, Z.T., Coceal, O., Castro, I.P., 2008. Large-eddy simulation of flows over random urban-like obstacles. Boundary-Layer Meteorol. 129, 1–23.
Yakhot, V., Smith, L.M., 1992. The renormalization group, the ε-expansion and derivation of turbulence models. J. Sci. Comput. 7, 35–61.
Yang, A.-S., Su, Y.-M., Wen, C.-Y., Juan, Y.-H., Wang, W.-S., Cheng, C.-H., 2016. Estimation of wind power generation in dense urban area. Appl. Energy 171, 213–230.
Yap, C.J., 1987. Turbulent Heat and Momentum Transfer in Recirculating and Impinging Flows (Ph.D. Thesis). Faculty of Technology, University of Manchester, United Kingdom.
Zanforlin, S., Letizia, S., 2015. Improving the performance of wind turbines in urban environment by integrating the action of a diffuser with the aerodynamics of the rooftops. Energy Procedia 82, 774–781.